



Parametric soil water retention models: a critical evaluation of expressions for the full moisture range

Raneem Madi¹, Gerrit Huibert de Rooij¹, Henrike Mielenz², and Juliane Mai^{3,a}

¹Dept. Soil System Science, Helmholtz Centre for Environmental Research – UFZ, Halle, Germany

²Institute for Crop and Soil Science, Julius Kühn-Institut – JKI, Braunschweig, Germany

³Dept. Computational Hydrosystems, Helmholtz Centre for Environmental Research – UFZ, Leipzig, Germany

^acurrently at: Dept. Civil & Environmental Engineering, Univ. of Waterloo, Waterloo, Canada

Correspondence: Gerrit Huibert de Rooij (gerrit.derooij@ufz.de)

Received: 12 April 2016 – Discussion started: 25 April 2016

Revised: 4 January 2018 – Accepted: 8 January 2018 – Published: 12 February 2018

Abstract. Few parametric expressions for the soil water retention curve are suitable for dry conditions. Furthermore, expressions for the soil hydraulic conductivity curves associated with parametric retention functions can behave unrealistically near saturation. We developed a general criterion for water retention parameterizations that ensures physically plausible conductivity curves. Only 3 of the 18 tested parameterizations met this criterion without restrictions on the parameters of a popular conductivity curve parameterization. A fourth required one parameter to be fixed.

We estimated parameters by shuffled complex evolution (SCE) with the objective function tailored to various observation methods used to obtain retention curve data. We fitted the four parameterizations with physically plausible conductivities as well as the most widely used parameterization. The performance of the resulting 12 combinations of retention and conductivity curves was assessed in a numerical study with 751 days of semiarid atmospheric forcing applied to unvegetated, uniform, 1 m freely draining columns for four textures.

Choosing different parameterizations had a minor effect on evaporation, but cumulative bottom fluxes varied by up to an order of magnitude between them. This highlights the need for a careful selection of the soil hydraulic parameterization that ideally does not only rely on goodness of fit to static soil water retention data but also on hydraulic conductivity measurements.

Parameter fits for 21 soils showed that extrapolations into the dry range of the retention curve often became physically more realistic when the parameterization had a loga-

rithmic dry branch, particularly in fine-textured soils where high residual water contents would otherwise be fitted.

1 Introduction

The pore architecture of the soil influences its hydraulic behavior, typically described by two curves: the relationship between the amount of water present in the soil pores and the matric potential (termed soil water characteristic or soil water retention curve), and the relationship between the hydraulic conductivity and either matric potential or water content (the soil hydraulic conductivity curve). Numerical solvers of Richards' equation for water flow in unsaturated soils require these curves as descriptors of the soil in which the movement of water should be calculated. Many parametric expressions for the retention curve and fewer for the hydraulic conductivity have been developed for that purpose (see the Supplement, Leij et al., 1997; Cornelis et al., 2005; Durner and Flühler, 2005; Khlosi et al., 2008; Assouline and Or, 2013).

A brief overview of retention curve parameterizations is given in the following while the references to the parameterizations in question are given in the Supplement and Sect. 2, where their equations are presented. The earliest developed parameterizations focused primarily on the wet end of the curve since this is the most relevant section for agricultural production. Numerical models were struggling with the discontinuity of the first derivative at the air-entry value. Observations with methods relying on hydrostatic equilibrium

(Klute, 1986, pp. 644–647) typically gave a more smooth shape around the matric potential where the soil started to desaturate as an artefact of the sample height, as was later demonstrated by Liu and Dane (1995). This led to the introduction of parameterizations that yielded a continuously differentiable curve.

The interest in the dry end of the retention curve was triggered by an increased interest in water scarcity issues (e.g., Scanlon et al., 2006; UN-Water, FAO, 2007; UNDP, 2006). For groundwater recharge under deep vadose zones, the dry end of the soil water retention curve affects both slow liquid water movement in film and corner flow (Tuller and Or, 2001; Lebeau and Konrad, 2010) and vapor phase transport (Barnes and Turner, 1998; de Vries and Simmers, 2002). The earlier parameterizations had an asymptote at a small (or at zero) water content. This often gave poor fits in the dry end, and several parameterizations emerged in which the dry branch was represented by a logarithmic function that reached zero water content at some point.

A nonparametric approach was advocated by Iden and Durner (2008). They estimated nodal values of volumetric water content from evaporation experiments and derived a smooth retention curve by cubic Hermite interpolation. They extrapolated the retention function to the dry range and computed a coupled conductivity function based on the Mualem model.

Liu and Dane (1995) were the first to point out that the smoothness of observed curves around the air-entry value could be an artefact related to experimental conditions. Furthermore, it became apparent that a particular parameterization that gave a differentiable curve led to unrealistically large increases of the soil hydraulic conductivity near saturation (Durner, 1994; Vogel et al., 2001). This was eventually linked to the nonzero slope at saturation (Ippisch et al., 2006), implying the existence of unphysically large pores with air-entry values up to zero. This led to the reintroduction of a discrete air-entry value.

Most of the parameterizations are empirical, curve-fitting equations (Kosugi et al., 2002). One exception is the very dry range, where measurement techniques are often not so reliable (e.g., Campbell and Shiozawa, 1992) and were not always employed. The proportionality of the water content in this range to the logarithm of the absolute value of the matric potential that has frequently been invoked conforms to the adsorption theory of Bradley (1936), which considers adsorbed molecules to build up in a film consisting of layers, with the net force of electrical attraction diminishing with every layer (Rossi and Nimmo, 1994).

The empirical power-law relationship between water content and matric potential introduced by Brooks and Corey (1964) was later given a theoretical foundation by Tyler and Wheatcraft (1990), who showed that the exponent was related to the fractal dimension of the Sierpinski carpet used to model the hierarchy of pore sizes occurring in the soil. The sigmoid shape of the Kosugi's (1996, 1999) reten-

tion curve was derived rigorously from an assumed lognormal distribution of effective pore sizes, making this the only parameterization discussed in this paper developed from a theoretical analysis.

Some soils have different types of pore spaces: one type appears between individual grains. Its architecture is determined by soil texture, and by the geometry of the packing of the individual grains. The second type appears on a larger scale: the soil may consist of aggregates (e.g., Coppola, 2000, and references therein), and the pore space between these aggregates is very different from those between the grains. Biopores formed by roots that have since decayed, soil fauna, etc. can also create a separate type of pore space. In shrinking soils, a network of cracks may form. The volume and architecture of these pore spaces are essentially independent of the soil texture (Durner, 1994), even though a certain texture may be required for these pores to form. In soils with such distinct pore spaces, the derivative of the soil water retention curve may have more than a single peak, and for this reason multimodal retention curves have been proposed, e.g., by Durner (1994) and Coppola (2000). Most of the parametric expressions for the soil water retention curve are unimodal though. Durner (1994) circumvented this by constructing a multimodal retention curve by summing up several sigmoidal curves of van Genuchten (1980) but with different parameter values. He presented excellent fits of bimodal retention functions at the price of adding three or four parameters, depending on the chosen parameterization. Priesack and Durner (2006) derived the corresponding expression of the hydraulic conductivity function. Romano et al. (2011) developed a bimodal model based on Kosugi's (1994) curve and derived the associated hydraulic conductivity function. Coppola (2000) used a single-parameter expression for the intra-aggregate pore system superimposed on a five-parameter expression for the inter-aggregate pores, thereby reducing the number of fitting parameters and the degree of correlation among these. The primary focus of this paper is on unimodal functions, but we briefly discuss three multimodal models as well.

The wealth of parameterizations for the soil water retention curve calls for a robust fitting method applicable to various parameterizations and capable of handling data with different data errors. These errors arise from the various measurement techniques used to acquire data over the full water content range. Parameter fitting codes are available (e.g., Schindler et al., 2015), but they do not fit the parameterizations focusing on the dry end. The first objective of this paper is to introduce a parameter fitting procedure that involves an objective function that accounts for varying errors, embedded in a shell that allows a wide spectrum of retention function parameterizations to be fitted.

The analysis by Ippisch et al. (2006) of the effect of the shape of the soil water retention curve on the hydraulic conductivity near saturation considered van Genuchten's (1980) parameterization in combination with Mualem's (1976) con-

ductivity model only. Iden et al. (2015) approached the same problem but only examined the conductivity curve. They too focused on the van Genuchten–Mualem configuration only. The analysis of Ippisch et al. (2006) could well have ramifications for other parameterizations. A second objective of this paper is therefore the development of a more general analysis based on Ippisch et al. (2006) and its application to other parameterizations of the retention and conductivity curves.

Several hydraulic conductivity parameterizations that relied only on observations of soil water retention data have been developed (see the reviews by Mualem, 1992 and Assouline and Or, 2013). Many of these consider the soil layer or sample for which the conductivity is sought as a slab of which the pore architecture is represented by a bundle of cylindrical tubes with a given probability density function (PDF) of their radii. This slab connects to another slab with a different pore radius PDF. By making different assumptions regarding the nature of the tubes and their connectivity, different expressions for the unsaturated hydraulic conductivity can be found (Mualem and Dagan, 1978). Raats (1992) distinguished five steps in this process: (1) specify the effective areas occupied by connected pairs of pores of different radii that reflect the nature of the correlation between the connected pore sizes; (2) account for tortuosity in one of various ways; (3) define the effective pore radius as a function of both radii of the connected pairs of pores; (4) convert the pore radius to a matric potential at which the pore fills or empties; and (5) use the soil water retention curve to convert from a dependence upon the matric potential to a dependence upon the water content. Only step 5 constitutes a direct effect of the choice of the retention curve parameterization on the conductivity curve. Choices made in steps 1–3 result in different conductivity curves associated with any particular retention curve parameterization.

These conductivity parameterizations give the hydraulic conductivity as a function of matric potential or water content relative to the value at saturation. They therefore require a value for the saturated hydraulic conductivity, either independently measured or estimated from soil properties. Assouline and Or (2013) review numerous expressions for the saturated hydraulic conductivity. Interestingly, approaches have emerged to estimate the saturated hydraulic conductivity from the retention curve parameters (Nasta et al., 2013; Pollacco et al., 2013, 2017).

The functions based on the pore bundle approach discussed by Mualem and Dagan (1978), Mualem (1992), and Raats (1992) that have found widespread application in numerical models can be captured by Kosugi's (1999) generalized model. In this paper, we limit ourselves to three parameterizations as special cases of Kosugi's general model, and discuss them in more detail in Sect. 2. In doing so, we add to the existing body of comparative studies of parametric retention curves by explicitly including the associated hydraulic conductivity curves according to these conductiv-

ity models. Papers introducing new parameterizations of the soil water retention curve as well as reviews of such parameterizations typically show the quality of the fit to soil water retention data (e.g., van Genuchten, 1980; Rossi and Nimmo, 1994; Cornelis et al., 2005; Khlosi et al., 2008). The role of these parameterizations is to be used in solutions of Richards' equation, usually in the form of a numerical model. Their performance can therefore be assessed through the water content and water fluxes in the soil calculated by a numerical Richards solver. This is not often done, one exception being the field-scale study by Coppola et al. (2009) comparing unimodal and bimodal retention curves and the associated conductivity curves in a stochastic framework on the field scale, for a 10-day, wet period. A third objective therefore is to carry out a numerical modeling exercise to examine the differences in soil water fluxes calculated on the basis of various parameterizations by the same model for the same scenario. By doing so, the inclusion of the conductivity curves in the comparison is taken to its logical conclusion by carrying out simulations for all possible combinations of retention and conductivity models.

Should the differences in the fluxes be small, the choice of the parameterizations can be based on convenience. If they are significant, even if the fits to the data are fairly similar, this points to a need for a more thorough selection process to determine the most suitable parameterization.

2 Theory

2.1 Hydraulic conductivity models and their behavior near saturation

Numerous functions have been proposed to describe the soil water retention curve, several of them reviewed below. Fewer functions exist to describe the soil hydraulic conductivity curve. When these rely on the retention parameters, one can use the retention curve to predict the conductivity curve. However, when both retention and conductivity data exist, a single set of parameters does not always fit both curves well, even if both sets of data are used in the fitting process. It may therefore be prudent to attempt to find a retention–conductivity pair of curves that shares a number of parameters that could be fitted on retention data only and has additional parameters that only occur in the expression for the hydraulic conductivity.

Various theoretical models exist to determine the unsaturated hydraulic conductivity K [$L T^{-1}$] as a function of matric potential h [L] or volumetric water content θ from the soil water retention curve (see the Appendix for a list of the variables used in this paper). Hoffmann-Riem et al. (1999) and Kosugi (1999) identified a generalized model that captured the two most widely used hydraulic conductivity models and several others. The formulation according to Ko-

sugi (1999) is as follows:

$$K(S_e) = K_s S_e^\tau \left(\frac{\int_0^{S_e} |h|^{-\kappa} dx}{\int_0^1 |h|^{-\kappa} dx} \right)^\gamma, \quad (1)$$

where the subscript s denotes the value at saturation, x is an integration variable, and γ , κ , and τ are dimensionless shape parameters. The degree of saturation S_e is defined as follows:

$$S_e(h) = \frac{\theta(h) - \theta_r}{\theta_s - \theta_r}, \quad (2)$$

where the subscript r denotes the irreducible value (≥ 0). After a change of variables this gives (Ippisch et al., 2006)

$$K(h) = K(h(S_e)) = \begin{cases} K_s S_e^\tau \left(\frac{\int_{-\infty}^{h(S_e)} |h|^{-\kappa} \frac{dS}{dh} dh}{\int_{-\infty}^{h_{ae}} |h|^{-\kappa} \frac{dS}{dh} dh} \right)^\gamma, & h \leq h_{ae} \\ K_s, & h \geq h_{ae}, \end{cases} \quad (3)$$

where h_{ae} [L] is the air-entry value of the soil and S denotes the degree of saturation moving between 0 and the actual value S_e . Note that the value of $S(h)$ and dS/dh are directly related to the soil water retention curve $\theta(h)$ through Eq. (2). Specific models can be found by fixing the parameters: Burdine’s (1953) model is obtained with $\gamma = 1$, $\kappa = 2$, and $\tau = 2$, the popular model of Mualem (1976) results when $\gamma = 2$, $\kappa = 1$, and $\tau = 0.5$, and the model of Alexander and Skaggs (1986) requires $\gamma = \kappa = \tau = 1$. Assouline and Or (2013) give parameter values for additional conductivity models. When any of these models are used, the soil water retention parameters can be used to predict the conductivity curve if no conductivity data are available and the saturated hydraulic conductivity can be estimated independently (see Jarvis et al., 2002, and references therein). Note that positive values of κ ensure that large pores (emptying at smaller values of $|h|$) contribute more to the overall hydraulic conductivity than small pores, which is a physically sound condition. Parameter γ should be positive as well. Negative values would lead to a switch of the numerator and denominator (which scales the numerator by its maximum value) in Eq. (1), which is illogical. Peters (2014) required that the conductivity curve monotonically decreases as the soil dries out and derived a minimal value of -2 for τ from that requirement. Indeed, negative values of this parameter have been reported (e.g., Schaap and Leij, 2000), even though the three predictive models mentioned above all have positive values of τ .

Driven by the occasionally unrealistic shape of Mualem’s (1976) hydraulic conductivity curve near saturation, Ippisch et al. (2006) rigorously analyzed the version of Eq. (3) specific to Mualem’s (1976) model. They concluded that the integrand must approach zero near saturation in order to prevent unrealistically large virtual

pores dominating the hydraulic conductivity of very wet soils, a point raised earlier by Durner (1994). We generalize their criterion for prohibiting excessively larger pores from dominating the conductivity near saturation for arbitrary parameter values (after converting dS/dh to $d\theta/dh$) by

$$\lim_{h \rightarrow 0} \left(|h|^{-\kappa} \frac{d\theta}{dh} \right) = 0. \quad (4)$$

This condition is automatically met by retention curves with nonzero air-entry values, but restricts the permissible value of κ if the retention curve has nonzero derivatives at saturation and couples it to this derivative.

Iden et al. (2015) argued that limiting the maximum pore size of the pore-bundle models that gave rise to models of the type of Eq. (1) eliminated the large pores that caused the excessively rapid rise of the hydraulic conductivity near saturation. By only modifying the conductivity function without changing the water retention function, a discrepancy emerges between the retention curve (which reflects the presence of unphysically large pores) and the conductivity curve (which does not). Retention curves with a distinct air-entry value maintain the desired consistency, at the price of having non-continuous derivatives. Computational tests by Ippisch et al. (2006) suggest that state-of-the-art numerical solvers of Richards’ equation are capable of handling this.

2.1.1 Critical evaluation of unimodal parametric functions of the soil water retention curve

The Supplement reviews 18 parameterizations of the soil water retention curve. Their derivatives are presented and used to verify the physical plausibility of the hydraulic conductivity near saturation according to Eq. (4). In this section only those equations that satisfy the criterion in Eq. (4) are presented, together with the associated hydraulic conductivity functions. For comparison, the most widely used parameterization is also included here. To facilitate cross-referencing between the Supplement and the main text, the equations lifted from the Supplement into the main text have the same number in the main text as in the Supplement.

The water retention function of Brooks and Corey (1964) is

$$\theta(h) = \begin{cases} \theta_r + (\theta_s - \theta_r) \left(\frac{h}{h_{ae}} \right)^{-\lambda}, & h \leq h_{ae} \\ \theta_s, & h > h_{ae}, \end{cases} \quad (S1a)$$

where λ is a dimensionless fitting parameter. This equation is referred to as BCO below. The analytical expression for the generalized $K(h)$ function (Eq. 3) for the water retention function of Brooks and Corey (1964) is

$$K(h) = \begin{cases} K_s \left(\frac{h(S_e)}{h_{ae}} \right)^{-\lambda\tau} \left[\frac{\left[\frac{\lambda(\theta_s - \theta_r) |h_{ae}|^\lambda}{\kappa + \lambda + 2} |h|^{-\kappa - \lambda} \right]_{-\infty}^h}{\left[\frac{\lambda(\theta_s - \theta_r) |h_{ae}|^\lambda}{\kappa + \lambda + 2} |h|^{-\kappa - \lambda} \right]_{-\infty}^{h_{ae}}} \right]^\gamma \\ = K_s \left(\frac{h_{ae}}{h} \right)^{\lambda(\gamma + \tau) + \gamma\kappa}, & h \leq h_{ae} \\ K_s, & h > h_{ae}. \end{cases} \quad (S1c)$$

Van Genuchten’s (1980) formulation is continuously differentiable:

$$\theta(h) = \theta_r + (\theta_s - \theta_r) (1 + |\alpha h|^n)^{-m}, \quad h \leq 0, \quad (S4a)$$

where α [L^{-1}], n , and m are shape parameters. Often m is set equal to $1 - 1/n$. This equation is denoted by VGN below. The hydraulic conductivity only exhibits acceptable behavior near saturation if $\kappa < n - 1$. For many fine and/or poorly sorted soil textures, n ranges between 1 and 2. Therefore, this restriction even excludes Mualem’s (1976) conductivity model when $n < 2$. For this reason we refrain from formulating analytical conductivity equations, even though van Genuchten (1980) presented such expressions for Burdine’s (1953) and Mualem’s (1976) models. Because of its popularity we will include it in the further evaluation anyway.

Ippisch et al. (2006) proposed to introduce an air-entry value and scale the unsaturated portion of VGN by its value at the water-entry value:

$$\theta(h) = \begin{cases} \theta_r + (\theta_s - \theta_r) \left(\frac{1 + |\alpha h|^n}{1 + |\alpha h_{ae}|^n} \right)^{-m}, & h < h_{ae} \\ \theta_s, & h \geq h_{ae}, \end{cases} \quad (S7a)$$

This equation is labeled VGA below. With the common restriction of $m = 1 - 1/n$, an expression can be found for $\kappa = 1$ that is slightly more general than Eq. (11) in Ippisch et al. (2006):

$$K(h) = \begin{cases} K_s \left(\frac{\theta - \theta_r}{\theta_s - \theta_r} \right)^\tau \left[\frac{1 - \left(1 - \frac{1}{B(h)}\right)^{\frac{n}{n-1}}}{1 - \left(1 - \frac{1}{C}\right)^{\frac{n}{n-1}}} \right]^\gamma \\ = K_s \left(\frac{B(h)}{C} \right)^\tau \left(\frac{1}{n} - 1 \right) \left[\frac{1 - \left(1 - \frac{1}{B(h)}\right)^{\frac{n}{n-1}}}{1 - \left(1 - \frac{1}{C}\right)^{\frac{n}{n-1}}} \right]^\gamma, & h < h_{ae} \\ K_s, & h \geq h_{ae}, \end{cases} \quad (S7c)$$

where

$$B(h) = 1 + |\alpha h|^n, \quad (S7d)$$

$$C = 1 + |\alpha h_{ae}|^n. \quad (S7e)$$

This equation can be used to define conductivity models according to Mualem (1976) and Alexander and Skaggs (1986), which both require that $\kappa = 1$.

Rossi and Nimmo (1994) preferred a logarithmic function over the Brooks–Corey power law at the dry end to better represent the adsorption processes that dominate water retention in dry soils, as opposed to capillary processes in wetter soils. They also implemented a parabolic shape at the wet end as proposed by Hutson and Cass (1987). Rossi and Nimmo (1994) presented two retention models, but only one (the junction model) permitted an analytical expression of the unsaturated hydraulic conductivity. Here, we modified the junction model by removing the parabolic expression for

the wet end of the retention curve in favor of the discontinuous derivative at the air-entry value:

$$\theta(h) = \begin{cases} 0, & h \leq h_d \\ \theta_s \beta \ln \left(\frac{h_d}{h} \right), & h_d < h \leq h_j \\ \theta_s \left(\frac{h_{ae}}{h} \right)^\lambda, & h_j < h \leq h_{ae} \\ \theta_s, & h > h_{ae} \end{cases}, \quad (S9a)$$

which is denoted as RNA below.

Rossi and Nimmo (1994) required the power law and logarithmic branches as well as their first derivatives to be equal at the junction point (θ_j, h_j) . With h_d fixed (Rossi and Nimmo found a value of -10^5 m for six out of seven soils and -5×10^5 m for the seventh), these constraints allow two of the five remaining free parameters to be expressed in terms of the other three. Some manipulation leads to the following expressions:

$$\lambda = \frac{1}{\ln|h_d| - \ln|h_j|}, \quad (S9c)$$

$$\beta = \lambda \left(\frac{h_{ae}}{h_j} \right)^\lambda. \quad (S9d)$$

This gives the fitting parameters h_{ae} , h_j , and θ_s . The associated conductivity model is

$$K(h) = \begin{cases} 0, & h \leq h_d \\ K_s S_e^\tau \left\{ \frac{\left[\frac{-\theta_s \beta}{\kappa} |h|^{-\kappa} \right]_{h_d}^h}{\left[\frac{-\theta_s \beta}{\kappa} |h|^{-\kappa} \right]_{h_d}^{h_j} - \left[\frac{\theta_s \lambda}{\lambda + \kappa} |h_{ae}|^\lambda |h|^{-(\lambda + \kappa)} \right]_{h_j}^{h_{ae}}} \right\}^\gamma \\ = K_s \left[\beta \ln \left(\frac{h_d}{h} \right) \right]^\tau \left[\frac{E(h)}{E(h_j) + F \left(|h_j|^{-\lambda - \kappa} - |h_{ae}|^{-\lambda - \kappa} \right)} \right]^\gamma, & h_d < h \leq h_j \\ K_s S_e^\tau \left\{ \frac{\left[\frac{-\theta_s \beta}{\kappa} |h|^{-\kappa} \right]_{h_d}^{h_j} - \left[\frac{\theta_s \lambda}{\lambda + \kappa} |h_{ae}|^\lambda |h|^{-(\lambda + \kappa)} \right]_{h_j}^{h_{ae}}}{\left[\frac{-\theta_s \beta}{\kappa} |h|^{-\kappa} \right]_{h_d}^{h_j} - \left[\frac{\theta_s \lambda}{\lambda + \kappa} |h_{ae}|^\lambda |h|^{-(\lambda + \kappa)} \right]_{h_j}^{h_{ae}}} \right\}^\gamma \\ = K_s \left(\frac{h_{ae}}{h} \right)^{\lambda \tau} \left[\frac{E(h_j) + F \left(|h_j|^{-\lambda - \kappa} - |h|^{-\lambda - \kappa} \right)}{E(h_j) + F \left(|h_j|^{-\lambda - \kappa} - |h_{ae}|^{-\lambda - \kappa} \right)} \right]^\gamma, & h_j < h \leq h_{ae} \\ K_s, & h > h_{ae}. \end{cases} \quad (S9e)$$

where

$$E(h) = \frac{\beta}{\kappa} (|h_d|^{-\kappa} - |h|^{-\kappa}), \quad (S9f)$$

$$F = \frac{\lambda}{\lambda + \kappa} |h_{ae}|^\lambda. \quad (S9g)$$

Fayer and Simmons (1995) used the approach of Campbell and Shiozawa (1992) to have separate terms for adsorbed and capillary-bound water. If the capillary binding is represented by a Brooks–Corey-type function, the retention model becomes

$$\theta(h) = \begin{cases} 0, & h \leq h_d \\ \theta_a \left(1 - \frac{\ln|h|}{\ln|h_d|} \right) + \left[\theta_s - \theta_a \left(1 - \frac{\ln|h|}{\ln|h_d|} \right) \right] \left(\frac{h_{ae}}{h} \right)^\lambda, & h_d < h < h_{ae} \\ \theta_s, & h \geq h_{ae}. \end{cases} \quad (S12a)$$

This expression is denoted FSB below. Note that this model is valid if h_{ae} does not exceed -1 cm. This condition will usually be met, unless the soil texture is very coarse. The corresponding conductivity model is

$$K(h) = \begin{cases} 0, & h \leq h_d \\ K_s S_e^\tau \left[\frac{\frac{|h_{ae}|^\lambda}{\ln|h_d|(\lambda+\kappa)} \left[\theta_a \left(\frac{\lambda+\kappa-1}{\lambda+\kappa} - \ln|h| \right) - \lambda(\theta_s - \theta_a) \ln|h_d| \right] |h|^{-\lambda-\kappa}}{\frac{|h_{ae}|^\lambda}{\ln|h_d|(\lambda+\kappa)} \left[\theta_a \left(\frac{\lambda+\kappa-1}{\lambda+\kappa} - \ln|h| \right) - \lambda(\theta_s - \theta_a) \ln|h_d| \right] |h|^{-\lambda-\kappa}} \right]_{h_d}^{h_{ae}} \right]^\gamma, & h_d < h \leq h_{ae} \\ K_s \left\{ \frac{\theta_a}{\theta_s} \left(1 - \frac{\ln|h|}{\ln|h_d|} \right) + \left[1 - \frac{\theta_a}{\theta_s} \left(1 - \frac{\ln|h|}{\ln|h_d|} \right) \right] \left(\frac{h_{ae}}{h} \right)^\lambda \right\}^\tau \left[\frac{\theta_a(G - \ln|h|) - I}{\theta_a(G - \ln|h_{ae}|) - I} |h|^{-\lambda-\kappa-J} \right]^\gamma, & h > h_{ae} \end{cases} \quad (S12c)$$

where

$$G = \frac{\lambda + \kappa - 1}{\lambda + \kappa}, \quad (S12d)$$

$$I = \lambda(\theta_s - \theta_a) \ln|h_d|, \quad (S12e)$$

$$J = [\theta_a(G - \ln|h_d|) - I] |h_d|^{-\lambda-\kappa}. \quad (S12f)$$

In the original equations as presented by Fayer and Simmons (1995), the adsorbed water content reached zero at h_d , while there is still some capillary-bound water at and below that matric potential, which is inconsistent. Furthermore, the terms with ratios of logarithms become negative for matric potentials below h_d . We therefore modified the original equations by setting the water content to zero below h_d .

In the Supplement we argue that most of the retention curves examined result in conductivity curves with physically unacceptable behavior near saturation, even though several of these expressions were derived with the explicit purpose of providing closed-form expressions for the hydraulic conductivity. Only the Brooks–Corey function (1964) (BCO, Eq. S1a), the junction model of Rossi and Nimmo (1994) without the parabolic correction (RNA, Eq. S9a), and the model of Fayer and Simmons (1995) based on the Brooks–Corey (1964) retention function (FSB, Eq. S12a) lead to an acceptable conductivity model with full flexibility (three free parameters: κ , γ , τ). The modified van Genuchten (1980) retention curve with a distinct air-entry value by Ippisch et al. (2006) (VGA, Eq. S7a) leads to a conductivity model with two fitting parameters if $m = 1 - 1/n$ because $\kappa = 1$.

2.1.2 Multimodal parametric functions of the soil water retention curve

The multimodal model of Durner (1994) is a weighted sum of van Genuchten's (1980) retention functions (Eq. S4a) with zero residual water content. The bimodal retention model of Coppola (2000) adds a rapidly decaying asymptotic function representing the aggregate pore space to Eq. (S4a), also with zero residual water content. Because they are derived from Eq. (S4a), neither multimodal retention model meets the criterion of Eq. (4). The asymptotic nature of the dry ends of

either multimodal retention model limits their usefulness under very dry conditions.

The bimodal model of Romano et al. (2011) consists of two of Kosugi's (1994) retention functions. Romano et al.'s expression for the derivative shows that at least for $\kappa = 1$ the criterion of Eq. (4) is met. The asymptotic dry end that was removed in the unimodal version by Khlosi et al. (2008) (Eq. S14a) remains though, limiting its applicability in dry soils. Khlosi et al.'s (2008) modification led to additional complications detailed in the Supplement, which is why we did not pursue this for the bimodal version. The remainder of the paper therefore only considers the unimodal models discussed above.

3 Materials and methods

3.1 Soil water retention and hydraulic conductivity data

3.1.1 Soil hydraulic data for the model simulations

Data were obtained from Schelle et al. (2013), who measured soil water retention curves for a range of soil textures (clay, silt, silt loam, and sand). They took undisturbed and disturbed samples of a silt loam, a silt, and a sand near Braunschweig (northern Germany) and of a clay near Munich (southern Germany). The retention data were measured on soil samples using different laboratory methods and cover the moisture range from saturation to near oven dryness at pF of approximately 7. For silt, silt loam, and sand they used data obtained by suction plates, pressure plates, and the dew-point method. For clay they used data from the evaporation method HYPROP[®] (UMS, 2015) (until pF 3), pressure plate and dew-point methods. Here, we trimmed the disproportionately large data set in the HYPROP[®] range by stratifying the data into intervals of 0.5 on the pF scale and then randomly picking one data point for each interval. This ensured an adequate sensitivity of the fit in the dry range for all textures. For some of the soil samples, hydraulic conductivity data were available, including the values at saturation (unpublished). Hydraulic conductivity data were obtained by the evaporation method according to Peters and Durner (2008).

Undisturbed samples of 4.0 cm height and 100 cm³ volume were used for the suction plate method, with 4 to 6 replicates for each soil. The HYPROP[®] setup worked with an undisturbed sample of 5.0 cm height and 250 cm³ volume (one replicate). The pressure plate method required disturbed samples of 1.0 cm height and 5.2 cm³ volume (5 or 6 replicates for each soil). The dew-point method worked with disturbed samples of approximately 10 g dry mass (7 to 24 replicates with pF values between 3.5 and 6.2). Additional details are given by Schelle et al. (2013).

The fitting routine uses the variance of the data error to determine the weighting factor each data point. We estimated

these on the basis of estimated measurement errors of water level readings, pressure gauges, sample masses, etc. Typically, the estimated standard deviation in the matric potential was 0.05 cm for $h = 0$; in the range of the sandbox apparatus (> -200 cm) it was 1.0 cm, and beyond that it was 10 cm. For the water content, the estimated standard deviation was 0.01 at saturation and 0.02 anywhere else. If we had specific information about the accuracy of the instruments and their gauges and scales, these values were adapted accordingly.

When the three conductivity parameters are set to the values dictated by Burdine (1953), Mualem (1976), or Alexander and Skaggs (1986), hydraulic conductivity curves can be derived from soil water retention data only, supplemented by an estimate for the saturated hydraulic conductivity. For the soils with available conductivity data we compared the hydraulic conductivity curves to the direct measurements.

3.1.2 Soil water retention data used to evaluate various retention curve parameterizations

We selected 21 soils from the UNSODA database (Nemes et al., 2001; National Agricultural Library, 2018). The database has relatively many records for sandy soils, and hardly any in heavy clays. The selected soils have no organic matter contents that would lead to considering them as organic soils, have texture data records that allow their texture class to be determined, are fairly uniformly distributed over the textures covered by the database, have data points on the main drying curve, and have measurements over a sufficiently wide range of matric potentials to allow retention curves to be fitted to them.

We classified the texture of the selected soils according to the USDA classification as well as the hydrologically oriented classification developed by Twarakavi et al. (2010). The latter distinguishes 12 texture classes, grouped in three sets (A, B, C) of four each (1 through 4). Soils with (nearly) 100 % sand, silt, or clay are classified as A1, B1, and C1, respectively. Numbers larger than 1 identify texture classes that must have at least two of the components sand, silt, and clay. B3 and C4 are the only categories that must have all three components. The differences with the USDA classification are considerable for clayey and silty soils, and we refer to Twarakavi et al. (2010) for full details. Figure 1 shows the distribution of the selected soils over the soil texture triangle.

3.2 Parameter fitting

3.2.1 Selected parameterizations

We fitted the original Brooks–Corey (BCO, Eq. S1a) and van Genuchten (VGN, Eq. S4a) parameterizations, and the derivatives thereof that do not lead to unrealistic hydraulic conductivities near saturation: FSB (Eq. S12a) and RNA (Eq. S9a), both of which emerged from BCO, and VGA (Eq. S7a), which emerged from VGN. Thus, BCO, FSB, and

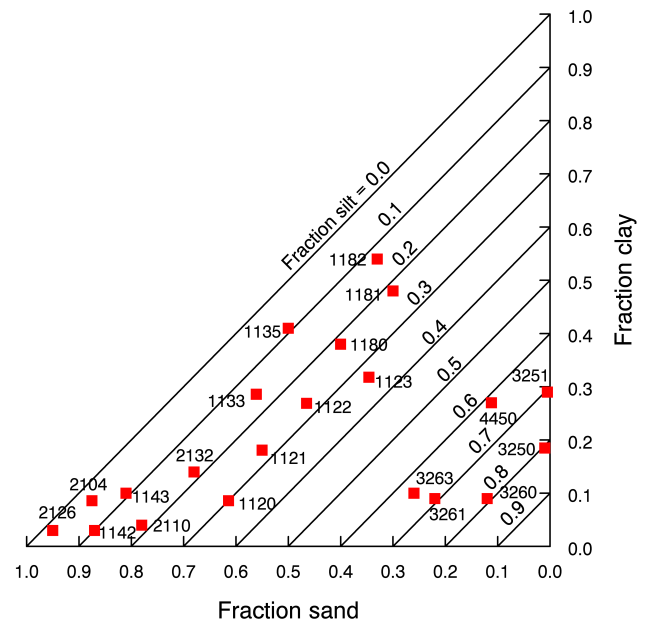


Figure 1. The textures of the soils used to test the fitting capability of selected soil water retention curve parameterizations. The numbers next to the data points are the identifiers used in the UNSODA database to distinguish individual soils.

RNA all have a power law shape in the mid-range of the matric potential (and for BCO over the full range below the air-entry value). The slope therefore monotonically increases with decreasing water content. VGN and VGA have a sigmoid shape and therefore are able to fit curves that have an inflection point. As Groenevelt and Grant (2004) pointed out, θ_r serves as the third required shape parameter for curves with an inflection point, frequently resulting in improbable values for this parameter. Table 1 shows the fitting parameters and their physically permitted range.

All three conductivity models are compatible with BCO, FSB and RNA. Burdine's (1953) and Mualem's (1976) conductivity models can be used with VGA. VGN does not meet the criterion of Eq. (4) but is very often used in conjunction with Mualem's conductivity model (1976). It was therefore included for comparison.

3.2.2 The objective function and its weighting factors

A set of parameters describing the soil water retention curve must be optimized to provide the best fit to an arbitrary number of data points. To do so, an objective function was minimized, construed by the sum of weighted squares of the differences between observed and fitted values. The fitted values depend on the parameter values in the parameter vector \mathbf{x} . Assume q_{θ} observation pairs of water content vs. matric head (h_i, θ_i). Here, θ_i denotes the i th observation of the volumetric water content, h_i [L] is the matric head at which that water content was observed (expressed as an equivalent

Table 1. The fitting parameters for five parameterizations, their physically permitted ranges, and their fitted values for four textures. The three-character parameterization label is explained in the main text.

Parameterization	Fitted parameter	Unit	Range	Texture			
				Silt	Sand	Clay	Silt loam
BCO	θ_r	–	$0-\theta_s$	0.000127	0.013300	0.000004	0.000015
	θ_s	–	θ_r-1	0.445	0.366	0.516	0.358
	h_{ae}	cm	$-\infty-0$	-21.426	-7.161	-50.577	-30.440
	λ	–	$0-\infty$	0.197	0.520	0.091	0.163
FSB	θ_s	–	θ_a-1	0.449	0.366	0.519	0.358
	θ_a	–	$0-\theta_s$	0.177	0.048	0.500	0.312
	h_{ae}	cm	h_d-0	-11.537	-11.508	-16.783	-11.668
	λ	–	$0-\infty$	0.254	0.719	0.152	0.364
RNA	θ_s	–	$0-1$	0.460	0.382	0.522	0.358
	h_{ae}	cm	h_j-0	-2.826	-1.884	-50.856	-30.250
	h_j	cm	h_d-h_{ae}	-2876	-359000	-49.882	-11641
VGA	θ_r	–	$0-\theta_s$	0.000133	0.012880	0.000019	0.000041
	θ_s	–	θ_r-1	0.461	0.366	0.514	0.358
	α	cm^{-1}	$0-\infty$	0.0197	0.8391	0.0055	0.0093
	n	–	$1-\infty$	1.252	1.511	1.127	1.219
	h_{ae}	cm	$-\infty-0$	-0.0015	-6.4626	-47.2530	-0.0081
VGN	θ_r	–	$0-\theta_s$	0.000025	0.013560	0.001160	0.000003
	θ_s	–	θ_r-1	0.461	0.370	0.509	0.360
	α	cm^{-1}	$0-\infty$	0.0200	0.1353	0.0042	0.0095
	n	–	$1-\infty$	1.251	1.528	1.127	1.219

water column), and $i \in \{1, 2, \dots, q_\theta\}$ is a counter. In the code, the assumed units are centimeters of water column for h and cubic centimeters of water per cubic centimeter soil for θ .

The definition of the objective function $F_R(\mathbf{x}_{p,R})$ at the R th iteration during the fitting operation is as follows:

$$F_R(\mathbf{x}_{p,R}) = \mathbf{w}_{\theta,R}^T \mathbf{d}_\theta(\mathbf{x}_{p,R}, \mathbf{x}_f) R \in \{1, 2, \dots, R_{\max}\}. \quad (5)$$

Here, \mathbf{d}_θ denotes a vector of length q_θ of squared differences between observations and fits that are functions of the fitted parameter values \mathbf{x}_p and the fixed (nonfitted) parameters in vector \mathbf{x}_f . Together, \mathbf{x}_p and \mathbf{x}_f constitute \mathbf{x} . Each squared difference is weighted. The weight factor vector is denoted by $\mathbf{w}_{\theta,R}$. Its dependence on the water content and iteration step is explained below. The superscript T indicates that the vector is transposed. To terminate infinite loops, the number of iterations is capped by R_{\max} .

For relatively wet soils ($0 > h > -100$ to -200 cm), measurement methods are available that create a hydrostatic equilibrium in a relatively large sample. In such cases h_i reflects the matric potential at the center of the sample but θ_i is that determined for the entire sample. The vertical variation of h results in a nonuniform water content, and the average water content of the sample (θ_i) may not be well represented by the water content corresponding to h_i . For these cases, the height of the sample can be specified on input. The code then

divides the sample into 20 layers, calculates h in the center of each layer, computes the corresponding water contents from $\mathbf{x}_{p,R}$, and averages these to arrive at an estimate of θ_i .

If and only if the standard deviation of the measurement error of the individual observations is known, a maximum-likelihood estimate of the soil hydraulic parameters can be obtained (Hollenbeck and Jensen, 1998). To ensure this, the weighting factors in vector $\mathbf{w}_{\theta,R}$ must be equal to the reciprocal of the variance of the measurement error. Note that this choice eliminates any effect of measurement units because the squared differences have the same units as the variances by which they are divided (Hollenbeck and Jensen, 1998). Only then can model adequacy be examined. A model is considered adequate if the residuals after parameter fitting are solely caused by measurement noise (Hollenbeck et al., 2000). Furthermore, only if these conditions are met can confidence intervals of fitted parameters be determined (Hollenbeck and Jensen, 1998). Even in that case, the contouring of the parameter space for permissible increases of the objective function required to determine the confidence region is not practically feasible for four or more parameters, and very laborious even for fewer parameters. A popular approximation based on the Cramer–Rao theorem was shown to be rather poor by Hollenbeck and Jensen (1998), so we refrained from implementing it. Instead we record the evolution of the

parameter values through the iterative process. Low information content (indicated by large random fluctuations of a parameter value), correlated parameters, and parameters trending towards a minimum or maximum permitted value can usually be diagnosed from such records.

Data points for a retention curve over the whole moisture range cannot be obtained by a single method. Furthermore, measurement errors occur in both h_i and θ_i . To accommodate this, the error standard deviations $\sigma_{h,i}$ and $\sigma_{\theta,i}$ for h and θ , respectively, can be provided individually for any data point i . To improve the performance of the fitting routine, the values of $\sigma_{\theta,i}$ are scaled to ensure their average equals 0.20, i.e., the same order of magnitude as θ . The values of $\sigma_{h,i}$ are then scaled by the same scaling factor. The weighting factor $w_{R,i}$ for observation θ_i during iteration R is as follows:

$$w_{R,i} = \sigma_{i,R}^*{}^{-2} = \left(\sigma_{h,i}^* \frac{d\theta}{dh} \Big|_{R,i} + \sigma_{\theta,i}^* \right)^{-2}, \quad (6)$$

where the asterisk denotes a scaled value. The subscripts i and R label data points and iteration steps as above. The gradient is determined from the R th fitted $\theta(h)$ relationship defined by $x_{p,R}$. Thus, the weighting factors are updated for every iteration.

In the code, the gradient is approximated by $\Delta\theta / \Delta h$ computed from the water contents at $h_i \pm \max(1 \text{ cm H}_2\text{O}, 0.01 \cdot h_i)$. For data points acquired at hydrostatic equilibrium, this would require 40 additional calls to the function that computes the θ corresponding to a given value of h , which would be rather inefficient. Instead, the water content is calculated for one virtual layer below and one above the sample. By subtracting the water content of the top (bottom) layer in the sample and adding the water content of the virtual layer below (above) the sample, the water content corresponding to $h_i + H/20$ ($h_i - H/20$) can be found, with H the sample height in centimeters. In this way, $\Delta\theta / \Delta h$ can be computed with only two additional calls to the function that defines the parameterized $\theta(h)$ relationship.

3.2.3 Parameter optimization by shuffled complex evolution (SCE)

The calibration algorithm employed here is the shuffled complex evolution algorithm introduced by Duan et al. (1992) with parameter adjustments of Behrangi et al. (2008). The strategy of this algorithm is to form out of $j + 1$ parameter sets, where j is the number of model parameters, so-called complexes (e.g., triangles in 2-D). Each vertex of the complex not only represents one of the $j + 1$ parameter sets but also the model's skill $F_R(x_{p,R})$ to match the observed data when it is forced with the according parameter set $x_{p,R}$. This skill is usually referred to as the objective function value of an objective to be minimized. The vertex with the worst skill or largest objective function value is subsequently perturbed in order to find a better substitute parameter set. This strategy

is repeated until the volume of the complex, i.e., the agreement of the parameter sets, is smaller than a threshold. To avoid that, the search gets stuck in a local optimum, and a number of Y complexes are acting in parallel. After a certain number of iterations the $Y \cdot (j + 1)$ vertexes are shuffled and newly assigned to Y complexes. The algorithm converges when the volume of all complexes is lower than a threshold which means that all $Y \cdot (j + 1)$ vertexes are in close proximity to each other. Infinite runs of the SCE are avoided by R_{\max} , but convergence should be the desired target for termination of the SCE.

The SCE algorithm used here is configured with two complexes each consisting of $(2j + 1)$ ensemble members. The different parameterizations we fitted had 3 to 5 fitting parameters. In each iteration, $j + 1$ parameters are randomly selected and the vertex with the worst skill is perturbed. The reflection and contraction step lengths in the Simplex method (e.g., Press et al., 1992, pp. 402–404) were set to 0.8 and 0.45, respectively. SCE seems to have an order of about $O(j^2)$. In our case it required between roughly 250 and 3000 model evaluations to find the optimal parameter set. For each parameter estimation run, three sets of initial guesses of the fitting parameters must be provided. The results of the three trials were compared to reduce the chance of accepting a local minimum of the objective function. The selection of SCE was based on its widespread usage in hydrological studies and according to a preliminary experiment where the SCE outperformed other algorithms like the simulated annealing (Kirkpatrick et al., 1983) and the Dynamically dimensioned search algorithms (Tolson and Shoemaker, 2007) in optimizing more than 80 analytical test functions with j ranging from 2 to 30.

3.3 Scenario study by numerical simulations

As stated in the Introduction, previous tests of parametric expressions of soil water retention functions mostly focused on the quality of the fit to direct observations of points on the water retention curve. Here, we will also examine how the various parameterizations affect the solution of Richards' equation by simulating water fluxes and soil water profiles for a scenario involving infiltration and evaporation. We set up a hypothetical 999-day scenario representative of a desert climate with prolonged drying, infiltration into dry soil, and redistribution after rainfall, permitting a comprehensive test of the parameterizations. We used the HYDRUS 1-D model version 4.xx (Šimůnek et al., 2013, <http://www.pc-progress.com/en/Default.aspx?hydrus-1d>) to solve Richards' equation in a 1-D soil profile. We permitted flow of liquid water as well as diffusive water vapor fluxes.

We considered an unvegetated uniform soil profile of 1 m depth, initially in hydrostatic equilibrium with -400 cm matric potential at the soil surface. The lower boundary condition was that of free drainage. In combination with the hydrostatic initial condition, this briefly caused some rapid

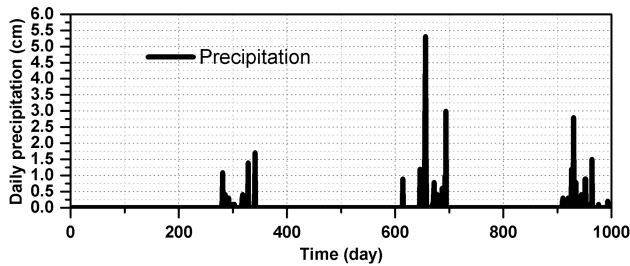


Figure 2. The record of daily rainfall sums from Riyadh city that was used in the numerical scenario study. Three rainfall clusters are visible. The largest daily rainfall amount (5.4 cm) fell on day 656. The observation period starts on 4 June 1993, and ends on 27 February 1996.

drainage immediately after the start of the simulation as the lowest part of the profile adapted to the unit gradient conditions in the two lowest nodes that the free drainage condition imposed. The upper boundary conditions were atmospheric (during dry periods: prescribed matric potential set to $-50\,000$ cm; during rain: prescribed flux density equal to the daily rainfall rate derived from observed daily sums). The weather data (daily rainfall and temperature) were taken from the NOAA database (<http://www.ncdc.noaa.gov/cdo-web/>, National centers for environmental information, 2017) for a station in Riyadh city (Saudi Arabia) between 4 June 1993 and 27 February 1996. In this period, spanning nearly 3 years, there were three clusters of rainfall events (Fig. 2). The second cluster was the heaviest with a maximum daily sum of approximately 5.4 cm on day 656. A prolonged dry spell preceded the first rainfall cluster. We used the first 250 days of this period as a “burn-in” period to minimize the effect of the initial condition on the calculated fluxes. This leaves a period of 751 days for analysis.

The simulation period involved large hydraulic gradients when water infiltrated a very dry soil, limited infiltration of small showers followed by complete removal of all water, and deeper infiltration after clusters of rainfall that delivered large amounts of water followed by prolonged periods in which flow of liquid water and water vapor occurred simultaneously. These processes combined permitted a comprehensive comparison of the various parameterizations. We were interested in the magnitude of the fluxes of liquid water and water vapor and the partitioning of infiltration into evaporation, storage change, and deep infiltration under various conditions, and the effect on these fluxes and storage effects of the choice of parameterization. We did not intend or desire to carry out a water balance study. Under semiarid conditions this would have required a much longer meteorological record, which was not available.

The various parameterizations are not implemented in HYDRUS. We therefore used the MATER.IN input file to supply the soil hydraulic property curves in tabular form to the model. The retention models BCO, FSB, and RNA permit-

ted all three conductivity models (Burdine, B; Mualem, M; and Alexander and Skaggs, AS) to be used. VGA only gives useful expressions for Burdine and Mualem. VGN only allows Mualem’s conductivity model. Thus, there are 12 combinations of retention and conductivity curves that we tested on four different textures, leading to 48 different simulations (and MATER.IN files) in total.

4 Results and discussion

4.1 Fitted parameters and quality of the fits for the soils used in the simulations

Table 1 presents the fitted parameters for all combinations of texture and parameterization for the soils used in the simulations. The parameter with the best-defined physical meaning is θ_s . All parameterizations give comparable values for it for each texture, which reflects the relatively narrow data clouds near saturation. The values of θ_r are relatively high for the three parameterizations in which it occurs. The air-entry values (h_{ae}) should increase (move closer to zero) from clay to silt loam to silt to sand, which is the case for BCO, FSB, and RNA, but not for VGA. The data in Fig. 3 support relatively similar values for all textures other than clay, which is somewhat surprising. RNA gives rather high values in silt and sand, and VGA does very poorly in sand and silt loam. The high value for h_{ae} for FSB in clay may be related somehow to the very high value of the maximum adsorbed water content θ_a , which we fixed close to θ_s . The value of θ_a for clay should be larger than that for silt loam, so it cannot be more than about 0.2 off though. The spread of h_j for RNA across the textures show that this parameter needs to be allowed to be fitted over its full range (between h_d and at least the minimum value of h_{ae}). Even with initial guesses that differed by several orders of magnitude, the fits were still quite consistent, so evidently these values are supported by the data and not an artefact.

In 3 of the 48 parameter estimation runs, the fits pushed one of the parameters to one of its bounds (even after expanding these to their physical limits), irrespective of their initial guess: FSB for clay (we fixed θ_a to 0.5), VGN for sand, and RNA for silt (we fixed θ_s on the basis of the data in both cases). For BCO and VGA in sandy soil, the code could not converge to a global minimum, indicated by the volume of the complexes, which exceeded the threshold. The fitted parameters should be viewed critically in these two cases.

The root mean square error (RMSE) of the fits (Table 2) illustrate why VGN has been very popular for over 3 decades. It gives the best fit in three cases (sand, silt, and silt loam) and the second-best fit in the fourth (clay). BCO performs poorest in three cases (sand, silt, and silt loam) and second-poorest in one (clay). The other three have varying positions, with no clearly strong or weak performers. FSB has the best performance in the finest soil (clay). The overall difference

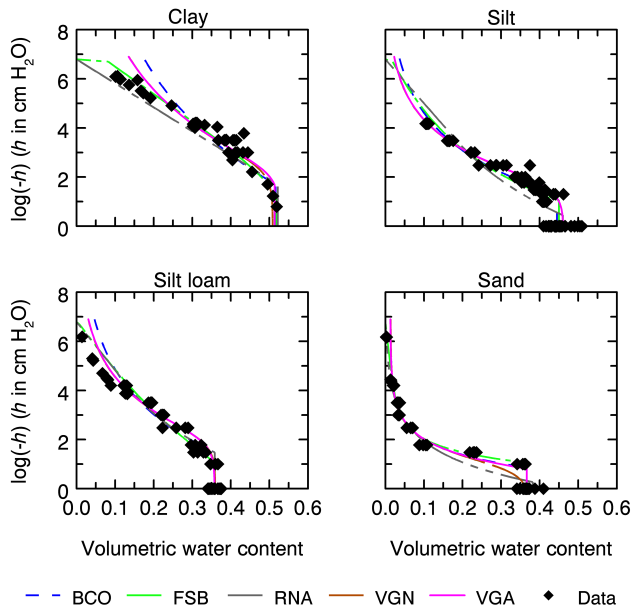


Figure 3. Observed and fitted retention curves for the different soil textures.

Table 2. Root mean square errors (RMSEs) for the different parameterizations.

Parameterization	Texture			
	Silt	Sand	Clay	Silt loam
BCO	0.1422	0.1164	0.1858	0.1122
FSB	0.1248	0.1163	0.1205	0.1068
RNA	0.0341	0.0130	0.2192	0.1101
VGA	0.0118	0.1164	0.1604	0.0412
VGN	0.0118	0.0111	0.1547	0.0411

in the RMSE values between textures reflects the different scatter in the underlying data clouds.

The soil water retention curves defined by the different parameterizations are plotted in Fig. 3. The models that were not developed with dry conditions in mind (BCO, VGA, and VGN) have relatively high water contents in the dry end of clay and silt loam. The logarithmic dry end of FSB and RNA eliminates this asymptotic behavior. The cutoff to zero of the FSB parameterization is quite strong in fine-textured soils. The fixed value of h_d (where the water content is zero) of RNA seems to be too small for clay while appearing to be adequate for the other textures.

In the intermediate range, all fits are close to one another. RNA underperforms in sand and silt compared to the others. In the wet range, the absence of an air-entry value in VGN results in a poor fit for sand. Here, the contrast between VGN and VGA is very clear. Overall, the inclusion of the water-entry value as a parameter seems beneficial to the fits. FSB has the most satisfactory overall performance.

For sand, silt, and silt loam, independent observations of $K(h)$ were available. The fits of Burdine’s (1953) and Mualem’s (1976) parameterizations based on retention data only were remarkably good for all parameterizations. The function of Alexander and Skaggs (1986) severely overestimated the hydraulic conductivity in all three cases, but very accurately described the slope of the curve for silt loam. Figure 4 demonstrates this for FSB, and the results for the other parameterizations were comparable.

4.2 Simulation results

For all simulations, the vapor flux within the profile was of little consequence compared to the liquid water flow. For that reason it will not be discussed in detail here. Vapor flow may play a larger role under more natural conditions with day–night temperature cycles and in the presence of plant roots.

4.2.1 Silt

We start the analysis by examining the flux at the bottom of the soil profile. Figure 5a–e shows all combinations of parameterizations of the retention and conductivity curves.

The early rainfall cluster event at around $t = 300$ days did not generate any bottom flux, and therefore only wetted up the soil profile. In doing so it increased the effect of the heavier rainfall around $t = 656$ days on the bottom flux.

For the individual parameterizations, Mualem and Burdine gave reasonably similar results in which the second and third rainfall cluster generated a little more downward flow for B than for M. In all cases, Alexander and Skaggs gave a more rapid response of a very different magnitude. Clearly visible is a sustained, constant flux leaving the column during prolonged dry periods for the AS conductivity curves. This is physically implausible.

Figure 5f shows the substantial effect of the parameterization of the water retention curve on bottom fluxes when the M-type $K(h)$ function is deployed. The results for B-type $K(h)$ were comparable. Different retention curves gave very different responses to the initial conditions (not shown), highlighting the need to add a sufficiently long lead time ahead of the target time window to the simulated time period. RNA’s response to the second and third rainfall clusters was about 2.4 times that of the others. At $h = -300$ cm (pF 2.48), K according to M is at least 5 times higher for RNA than for the rest, while the water content at that matric potential and higher values is relatively small (Fig. 3c). Thus, infiltrated water was transported downward with relative ease, giving rise to the relatively high bottom fluxes and low evaporation rates that were computed for RNA (Figs. 5f, 6f). The parameterizations other than RNA behaved rather similarly, except for the fact that VGA responded much faster to a change in the forcings than the other parameterizations.

Figure 5g shows the similar comparison of all parameterizations for the AS-type $K(h)$ function. The response to rain-

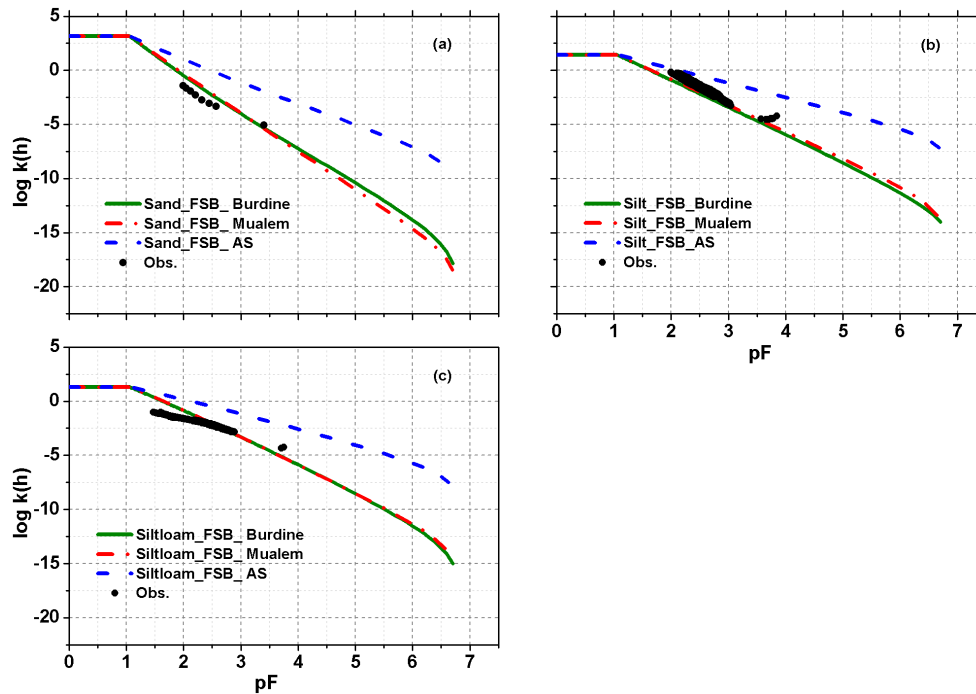


Figure 4. The observed and fitted hydraulic conductivity curve according to Burdine (1953), Mualem (1976), and Alexander and Skaggs (1986) using the fitted parameters of the Fayer and Simmons soil water retention curve (1995) for (a) sand, (b) silt, and (c) silt loam. The units of K are centimeters per day (cm d^{-1}).

fall was very fast and short-lived, which seems improbable for a silt soil that is far from full saturation. The nonphysical bottom flux during dry periods (especially for VGA), the slow calculation times (half as fast as the others) with the time step always at the smallest permitted value, and non-negligible mass balance errors all point to numerical problems associated with AS.

The evaporative flux was nearly identical for B and M conductivity functions (Fig. 6a–c). Since their bottom fluxes differed, this necessarily implies that the storage in the soil profile must also be different for B and M. The AS parameterization gave a much more spiky response of evaporative flux to rainfall than B or M, with zero evaporation most of the time (Fig. 6a–d). In terms of cumulative evaporation, AS responded more strongly to the second rainfall cluster around $t = 650$ days (Fig. 6a–c). Overall, the effect of the conductivity function on the relative differences in evaporation was less pronounced than on the relative differences in the bottom flux. The same was true for the parameterization of the retention curve, as demonstrated by the relatively similar shapes of the curves in Fig. 6f and g.

Given the nonphysical behavior of the bottom flux of AS for VGA in particular (Fig. 5d), we also examined the infiltration. We first compare infiltration for VGA with M- and AS-type conductivity (Fig. 7a) and clearly see the zero infiltration for VGA during periods without rain contrasted to the impossible nonzero infiltration rates for AS during dry spells.

For the other water retention parameterizations in combination with AS, the effect is less pronounced (Fig. 7b). Still, the AS conductivity should be used with care and the results and mass balance checked.

Table 3 summarizes the bottom and evaporative fluxes. For evaporation, the differences are inconsequential except for the markedly low values for RNA. For the bottom flux, the difference between B and M is small enough to be within the margin of error for typical applications. The effect of the parameterization of the retention curve is an order of magnitude between the smallest bottom flux (for VGA) and the largest (for RNA).

4.2.2 Sand

The relationship between the bottom (Fig. 8) and evaporative fluxes (Fig. 9) as generated by the various parameterizations for the sandy soil were comparable to those for silt, and the analysis applied to the silt carries over to sand. The bottom fluxes in sand responded faster and with less tailing than in silt, and the third rainfall cluster near the end of the simulation period produced a clear signal (Fig. 8).

The FSB (Fig. 8b) and RNA (Fig. 8c) parameterizations were both in their logarithmic dry range when bottom fluxes occurred, and both gave comparable values. BCO is not well adapted for dry conditions, and this is reflected by a bottom flux that is 4 times lower than the others (Fig. 8g).

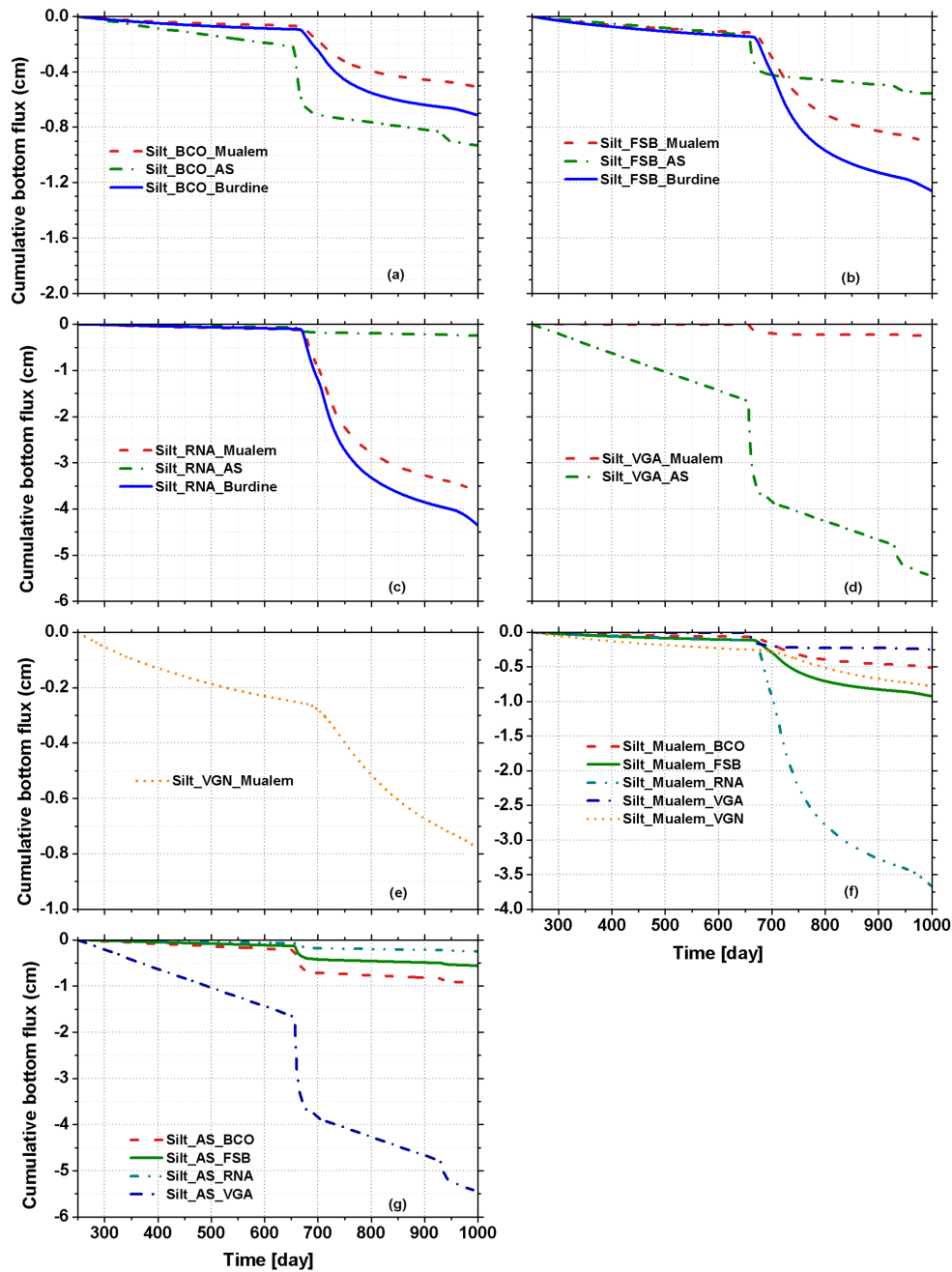


Figure 5. The cumulative bottom fluxes leaving a silt soil column for the different combinations of soil water retention curve and hydraulic conductivity parameterizations. Panels (a) through (e) present the results for the indicated retention parameterizations (see Table 1). Panels (f, g) organize the results according to the conductivity function: either Mualem (1976) (f) or Alexander and Skaggs (1986) (g).

The bottom fluxes for BCO and FSB with AS-type $K(h)$ are similar (Fig. 8h), in stark contrast to the bottom fluxes based on B (Fig. 8f) and M (Fig. 8g) for these parameterizations. The similarity in the fluxes for AS reflect the facts that the evaporative fluxes (occurring in the wet range, where BCO and FSB both have Brooks–Corey retention curves) are very similar and the spiky response typical for AS results in only a small difference in storage between BCO and FSB.

Consequently, the bottom flux, as the only remaining term of the water balance, cannot differ strongly between BCO and FSB. The difference in the bottom fluxes generated for VGN and VGA with M-type $K(h)$ (Fig. 8g) is even more extreme than in case of the silty soil.

For both B and M conductivity functions, the evaporation (Fig. 9a and b) and the bottom flux (Fig. 8a, f, and g) for BCO differed from the other parameterizations. These dif-

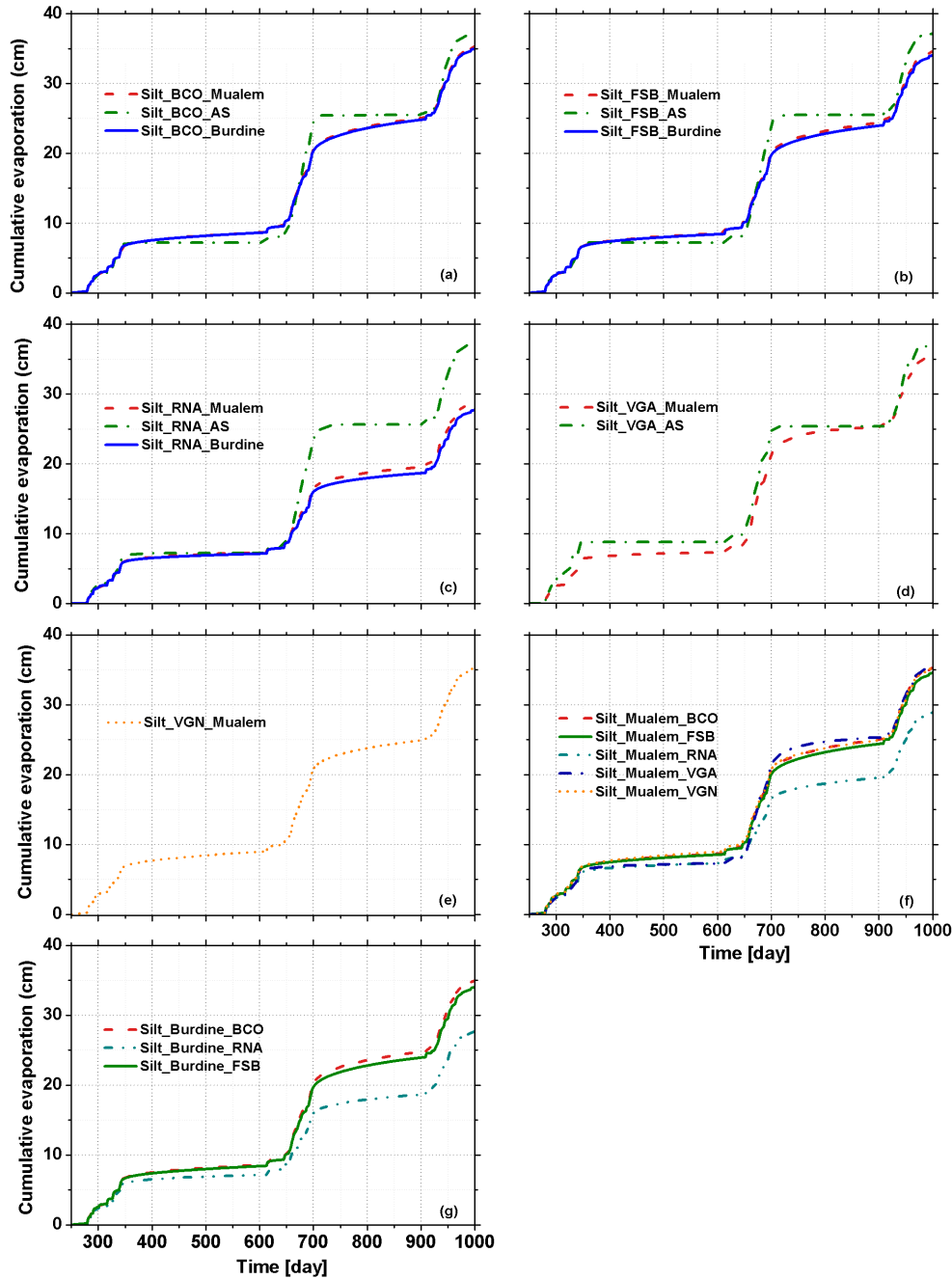


Figure 6. Cumulative evaporation from a silt soil column for the different combinations of soil water retention and hydraulic conductivity parameterizations. Panels (a) through (e) present the results for the indicated retention parameterizations (see Table 1). Panels (f, g) organize the results according to the conductivity function: either Mualem (1976) (f) or Burdine (1953) (g).

ferences seem to have been dominated by the complementary responses of evaporation and bottom fluxes to the rainfall events around $t = 656$ days. BCO converted roughly 5–7 cm more of this rainfall to evaporation than the other parameterizations, for both B and M. Therefore, less water was available for downward flow, resulting in a cumulative bot-

tom flux for BCO that was roughly 6 to 8 cm smaller than for the other parameterizations.

The AS-type $K(h)$ function again gave a spiky response (Fig. 9a). Nevertheless, the differences in the evaporation and the bottom flux compared to those of B and M are not very large. The bottom fluxes resulting from rainfall events were

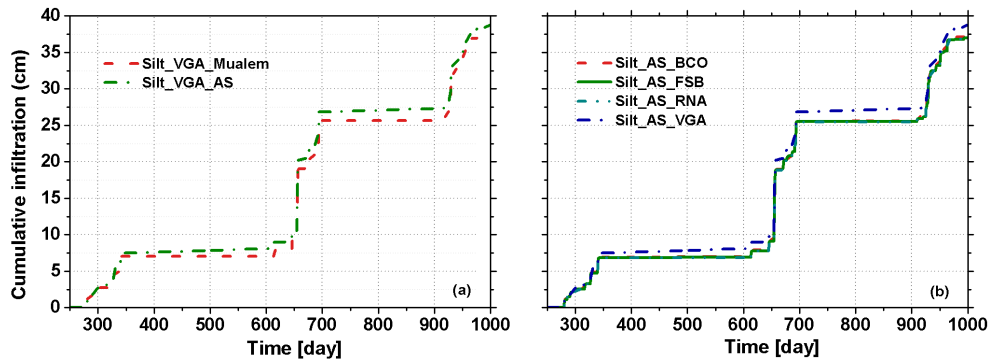


Figure 7. Cumulative infiltration in a silt profile for the VGA parameterization (see Table 1) with conductivity functions according to Mualem (1976) and Alexander and Skaggs (1986) (a) and four different parameterizations for the retention curve (see Table 1) with the Alexander and Skaggs conductivity function (b).

Table 3. Cumulative bottom and evaporative fluxes (positive upwards) for silt from day 281 (the start of the first rainfall) onwards for Burdine and Mualem conductivity functions with the different parameterizations. The hydraulic conductivity at $h = -300$ cm (the initial condition at the bottom) is also given.

Parameterization	Cumulative bottom flux (cm)		Cumulative evaporation (cm)		$K(-300)$ (cm d ⁻¹)
	Burdine	Mualem	Burdine	Mualem	Mualem
BCO	-0.70	-0.500	34.147	34.445	0.00080
FSB	-1.240	-0.910	33.219	33.736	0.00147
RNA	-4.337	-3.650	27.046	28.184	0.00702
VGA	-	-0.248	-	34.956	0.00014
VGN	-	-0.744	-	34.359	0.00119

considerably smaller for RNA than for the other parameterizations.

Coarse-textured soils have the sharpest drop in the hydraulic conductivity as the soil desaturates. We therefore used the result for the sandy column to study the relationship between the matric potential at the bottom of the column and the bottom flux in order to evaluate water fluxes in dry soils. The free drainage lower boundary condition ensures there is always a downward flux that is equal to the hydraulic conductivity at the bottom at any time. Particularly for coarse soils this can still lead to negligible bottom fluxes for considerable periods of time. We first consider FSB and RNA, these being the parameterizations specifically developed to perform well in dry soils.

The difference in matric potentials between FSB and RNA is immediately clear from Fig. 10a, b and 11a, b. The effect of the conductivity function is manifest by including Figs. 10c and 11c in the comparison. The effect of the first rainfall cluster is visible in the matric potential in all cases (Figs. 10 and 11), but not enough to generate a significant flux. A flux through the lower boundary first occurs when the matric potential there exceeds (i.e., becomes less negative than) -70 cm for FSB (Fig. 10a and b) and -30 cm for RNA (Fig. 11a and b).

The second rainfall cluster at $600 < t < 700$ days did not rely on prewetting: it produced a bottom flux no matter how dry the soil was. The third rainfall cluster around day 930 probably would not have generated a bottom flux for B- and M-type $K(h)$ functions, had the previous rainfall cluster not prewetted the soil. Note that the previous rainfall affects matric potentials at 1 m depth for several hundreds of days for B- and M-type conductivity functions, but only for a few months at most for AS.

The AS-type $K(h)$ function gave such rapid responses that only the second flux event at about 694 days was a result of recent prewetting at $t \approx 656$ days (Figs. 10c and 11c). Despite the very different matric potentials at the bottom, the cumulative bottom fluxes produced by a single rainfall cluster generated by FSB and RNA were quite similar for B and M and only somewhat larger for AS (Figs. 10 and 11).

The AS conductivity function led the soil to dry out so completely that the atmospheric matric potential during dry spells was reached at 1 m depth in a few months (Figs. 10c and 11c). This seems unrealistic, and seems to be related to the significant overestimation of the unsaturated hydraulic conductivity by AS evidenced in Fig. 4.

For comparison, the bottom matric potentials and fluxes are given for BCO as well (Fig. 12). They are very different and, given the poor suitability of BCO for dry soils and the

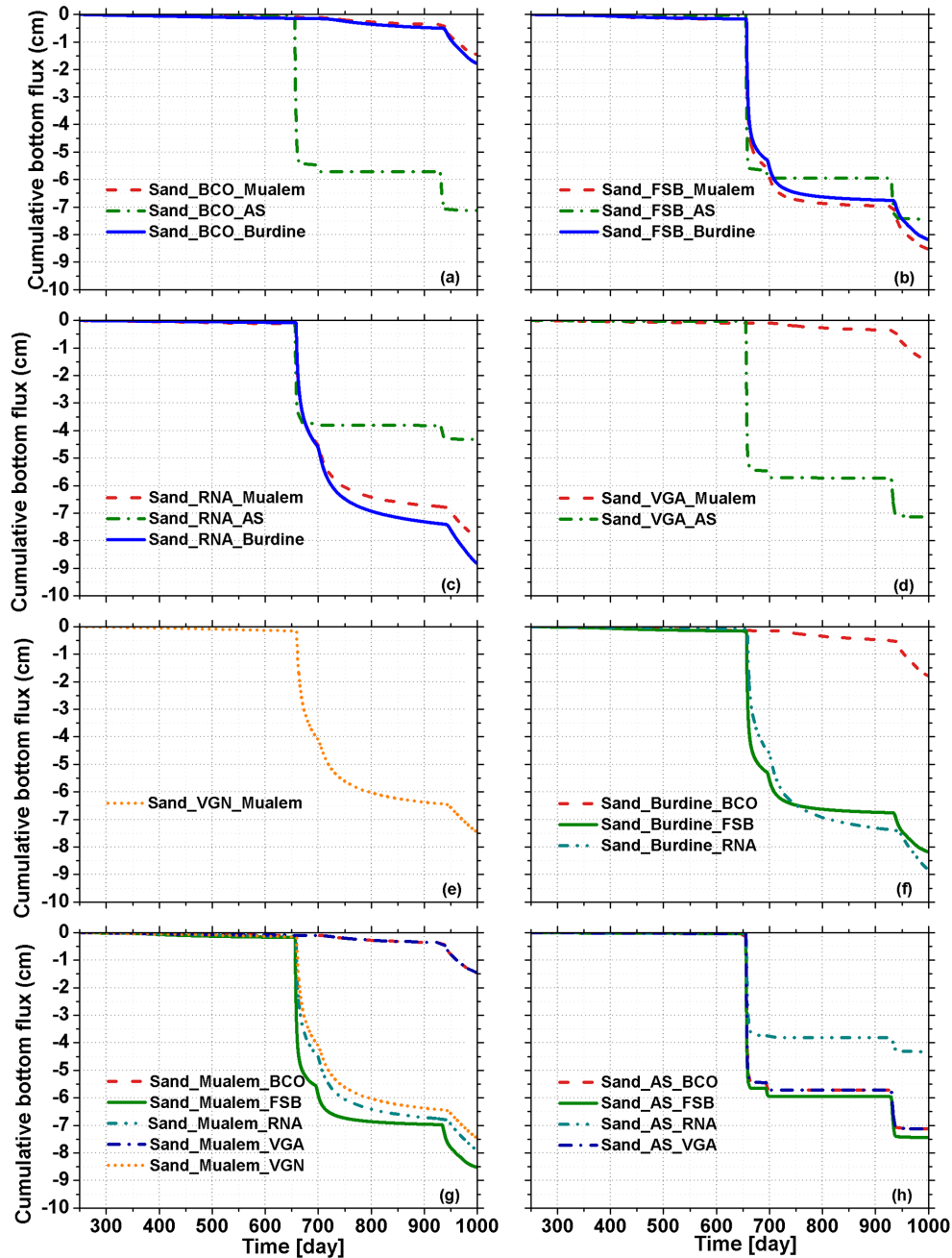


Figure 8. As in Fig. 5, but for a sandy soil column. Unlike Fig. 4, the results of Burdine’s (1953) conductivity curve are shown (f).

poor fitting performance, probably incorrect. The differences between the parameterizations illustrate the need to carefully consider the suitability of the parameterization for the intended purpose.

4.2.3 Silt loam and clay

The bottom fluxes from the clay and the silt loam soil for all combinations of parameterizations for the soil water retention and hydraulic conductivity curves were similar to those

for the silt soil (Figs. 13 and 16), with two notable exceptions: for RNA, there was a much more damped response to the rainfall around $t = 656$ days for either the B- or the M-type $K(h)$ function (Fig. 13c), in comparison to the rapidly increasing bottom flux in silt. In clay, there was virtually no response anymore (Fig. 16c). In general, the bottom fluxes for all parameterizations displayed comparable behavior with the exception of those with AS-type $K(h)$ functions (Figs. 13 and 16).

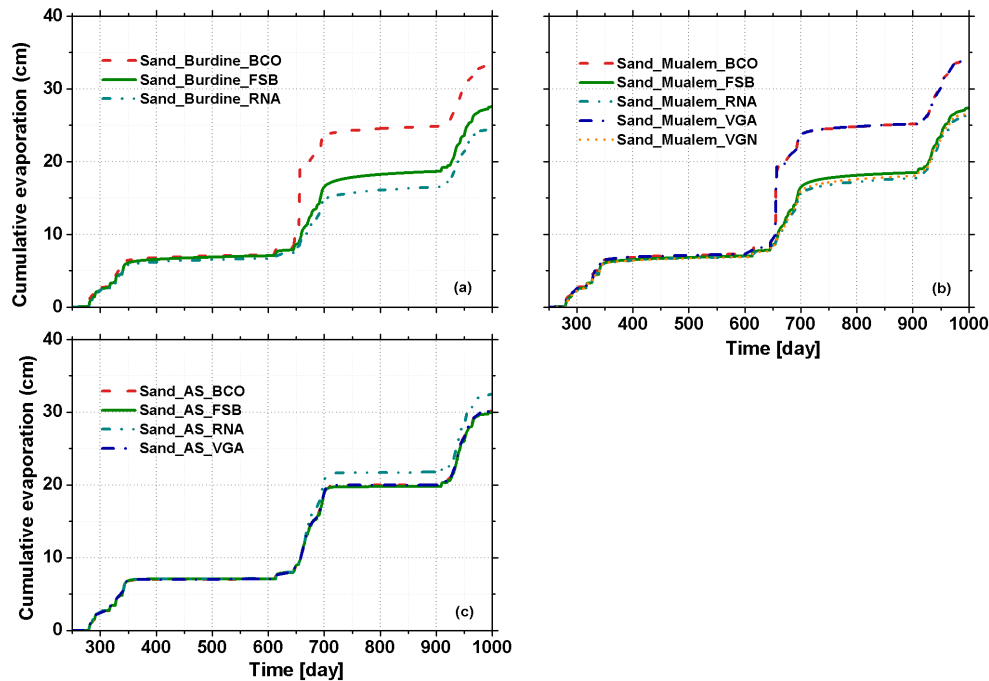


Figure 9. Cumulative evaporation from a sandy profile for the different combinations of retention curve parameterizations (see Table 1) and hydraulic conductivity functions: Burdine (1953) (a), Mualem (1976) (b), or Alexander and Skaggs (1986) (c).

The behavior of the evaporative fluxes from the silt loam and the clay soil for all combinations of parameterizations for the soil water retention and hydraulic conductivity curves was essentially similar to that for the silty soil (Figs. 14 and 17). The main difference was the less gradual response of the evaporation for VGA, particularly for clay, which was, in fact, rather similar to the notoriously spiked response of the AS-type conductivity function. The relative amounts of evaporation of the various parameterizations varied from one texture to another.

For AS in combination with the VGA retention curve, there was significant infiltration during periods of zero rainfall (Figs. 15 and 18). This numerical artefact led to erroneous simulations of the bottom flux. This is the most significant occurrence of mass balance errors that plague the simulations with AS-type $K(h)$ functions in silt loam and clay, as they did in silt. Evidently, the AS parameters for the $K(h)$ curve cause numerical problems in fine-textured soils.

4.3 Fits for a wide range of textures

The fits for the clayey soils selected from the UNSODA database (Fig. S1, first panel) show that with data ranging to $pF \approx 4$, data points in the drier region would have helped guide the fitting process. VGA and VGN produced good fits but struggled with high residual water contents, as did BCO. We modified FSB by requiring that the capillary-bound water content goes to zero when the adsorbed water content does, a modification of the original equation by Fayer and Sim-

mons (1995). The cutoff value of the matric potential was clearly too small for these fine-textured soils, and an unrealistic jump to zero water content occurred for the C2 and C4 soils with nos. 1122, 1123, 1135, 1181, and 1182 in the UNSODA database. The matric potential at oven dryness evidently needs to be extremely low for soils with high clay content.

Rossi and Nimmo (1994) fixed the matric potential in their parameterization at which the water content became zero. The fits for the soils used in the simulations showed that fixing h_d for RNA did not always give satisfactory fits in the dry range, and we therefore made h_d a fitting parameter. Supplement Fig. S1 (first panel) shows that this parameter may need a large lower boundary, similar to FSB: the maximum value ($pF = 10$) still gave poor fits for some of the fine-textured soils (soils with nos. 1122 and 1123, both C4 in Twarakavi et al.'s (2010) classification, in which the category is centered roughly around the point where sand, silt, and clay all contribute one-third to the total mineral soil).

Soil 1180 (Fig. S1, first panel) had a large discrepancy between the porosity and the unsaturated water contents. The effect on the shape of FSB points to the effect of the weighting factors: the accuracy of the porosity was assumed to be higher than that of the water content measurements. Because the weighting factors of the data points are inversely proportional to the measurement error as quantified by its estimated standard deviation, the outlier was given more weight in this case. If weighting factors are manipulated to improve

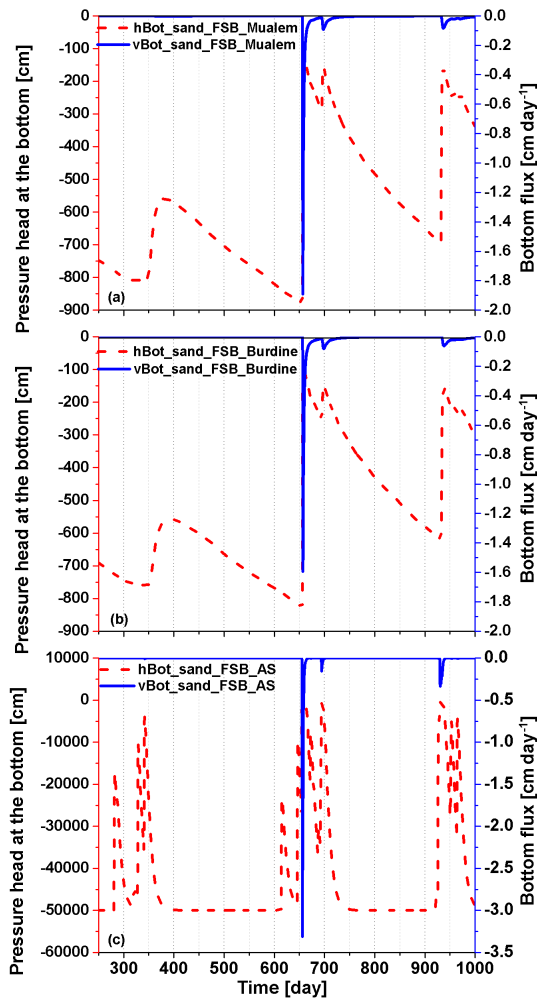


Figure 10. Pressure head h_{Bot} and flux density v_{Bot} at the bottom of the sand column for the FSB parameterization (see Table 1) and the conductivity functions of Mualem (1976) (a), Burdine (1953) (b), and Alexander and Skaggs (1986) (c).

the quality of the fit, the fitted parameter values can no longer be qualified as maximum likelihood estimates.

For silty soils (Fig. S1, second panel), the fits were generally good, with some evidence that the fitted residual water contents were somewhat high for some soils (3260, 3261). The extrapolations to zero water content by FSB and RNA appeared plausible even though they differed significantly in some cases (3251, 4450), highlighting the desirability of data points in the dry range.

For sandy soils with some clay and/or silt (A3 and A4, Fig. S1, third panel), residual water contents for BCO, VGN, and VGA were often large (1120, 1143, 2110, 1133). When the data range was limited (below $pF \approx 4$), considerable extrapolation was required. In most cases, FSB and RNA did so better than VGN and VGA. If there is a discrepancy between the porosity and near-saturated water contents (1121, 1143, and 2110), BCO and FSB tended to shift their saturated

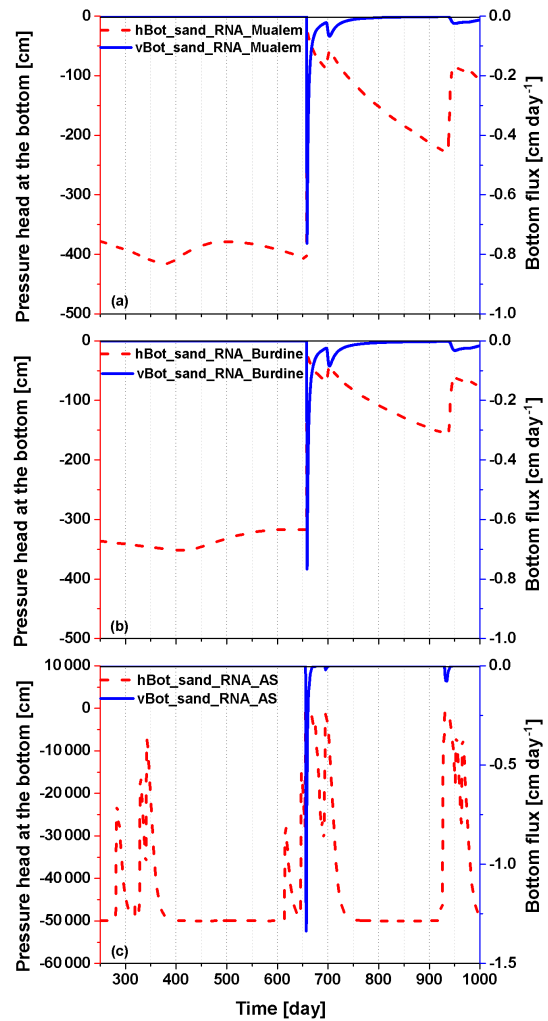


Figure 11. As in Fig. 10, but for the RNA parameterization (see Table 1).

branches towards the porosity, because of the higher weight assigned to this data point.

For sandy soils (A1 and A2, Fig. S1, fourth panel), the fits were good if the data covered the full water content range. In all cases, VGA and VGN fitted the residual water content close to driest data point, which is very unrealistic if the dry range was not covered (1142).

The RMSE values in Tables S5–S8 in the Supplement reflect the observations based on the curves above. If the curves have a clear inflection point, which is the case for the sands and some of the silty soils, the van Genuchten-based curves (VGN and VGA) outperform the Brooks–Corey-based curves (BCO, FSB, RNA) (Tables S6–S8). With two exceptions in clays and silty soils, VGA and VGN have very similar RMSE values. As discussed above, the upper limit of h_d in the RNA parameterization was very high but still too small for clayey soils, leading to very poor RMSE values for RNA in a few cases (Table S5).

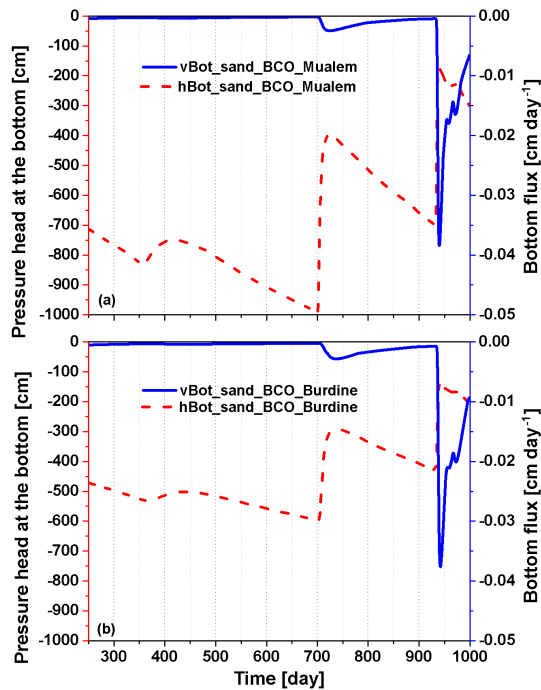


Figure 12. As in Fig. 10, but for the BCO parameterization (see Table 1).

For the fits of the four soils used for the simulation and the 21 soils, sets of three optimizations were independently run for all five parameterizations, with initial guesses that covered the full range over which the parameters were allowed to vary. In about a quarter of the cases we found no more than a single acceptable fit, and we ran these again with other sets of initial guesses (again widely different from one another) and/or expanded parameter ranges. For only two of the 125 fitted parameter sets did this procedure not lead to convincing convergence.

In none of the cases did the three independent runs yield parameter estimates that differed by more than 10 % while the sum of squares of the fits differed by less than 10 %, even though in all cases the initial guesses were very different, thereby ensuring that the starting points of the different searches were located in completely different regions of the parameter space. We take this as evidence of the absence of parameter correlations, since one would expect correlated parameters to vary over a considerable range, with the RMSE of different combinations of parameter values remaining nearly constant. We found that the fitted values obtained from the different runs were very similar, with an occasional outlier in a local minimum with a considerably larger RMSE.

In order to determine the correlation matrix of the fitted parameters correctly, a Markov Chain–Monte Carlo approach would be required for each of the 125 combinations of soils and parameterizations. Given the lack of evidence that signif-

icant correlations exist, we considered this beyond the focus of and the computational resources available for this work.

Some of the data sets displayed multimodality. None of the parameterizations we tested can account for that, which is why we did not examine this further in this paper. If one wishes to reproduce this by summing several curves of the same parameterization but with different parameter values (advocated by Durner, 1994), one needs a sigmoidal curve. If physically realistic conductivity curves near saturation are deemed desirable, VGA is the only viable parameterization for this purpose among those evaluated in this paper.

4.4 General ramifications

We found that 14 out of 18 parameterizations of the soil water retention curve were shown to cause nonphysical hydraulic conductivities when combined with the most popular (and effective) class of soil hydraulic conductivity models. For one of these cases (VGN), Ippisch et al. (2006) demonstrated convincingly that their alternative (VGA) significantly improved the quality and numerical efficiency of soil water flow model simulations, and our simulations confirmed the profound effect of this modest modification on the model results. We hope that the general criterion we developed for verifying the physical plausibility of the near-saturated conductivity will be used in the selection of suitable soil hydraulic property parameterizations for practical applications of numerical modeling of water flow in soils, and likewise will be of help in improving existing parameterizations (as we have done in a few cases here) and developing new ones.

Replacing the residual water content in a retention curve parameterization by a logarithmic dry branch generally improved the fits in the dry range for many soils. If data in the dry range were lacking, the logarithmic extension provided a physically realistic extrapolation into the dry range, but the spread between the different fits showed the level of uncertainty in this extrapolation caused by the limited range of the data. The cutoff to zero water content of FSB could be excessive for fine-textured soils, but this is only a problem if the soil actually so far that it reaches h_d . For RNA, adequate fits in the dry range require that the matric potential at which the water content reaches zero is to be treated as a fitting parameter. With the added flexibility of this fourth fitting parameter, RNA emerged as a very versatile parameterization, producing mostly good fits for a wide range of textures. Nevertheless, its lack of an inflection point was occasionally a limitation.

The ability of both Burdine's (1953) and Mualem's (1976) models of the soil hydraulic conductivity function to predict independent observations of the soil hydraulic conductivity curve on the basis of soil water retention parameters fitted on water content data only is reasonably good, at least for the limited data available to test this. The conductivity model of Alexander and Skaggs (1986) overestimated the conductivity of the soils for which independent data were available.

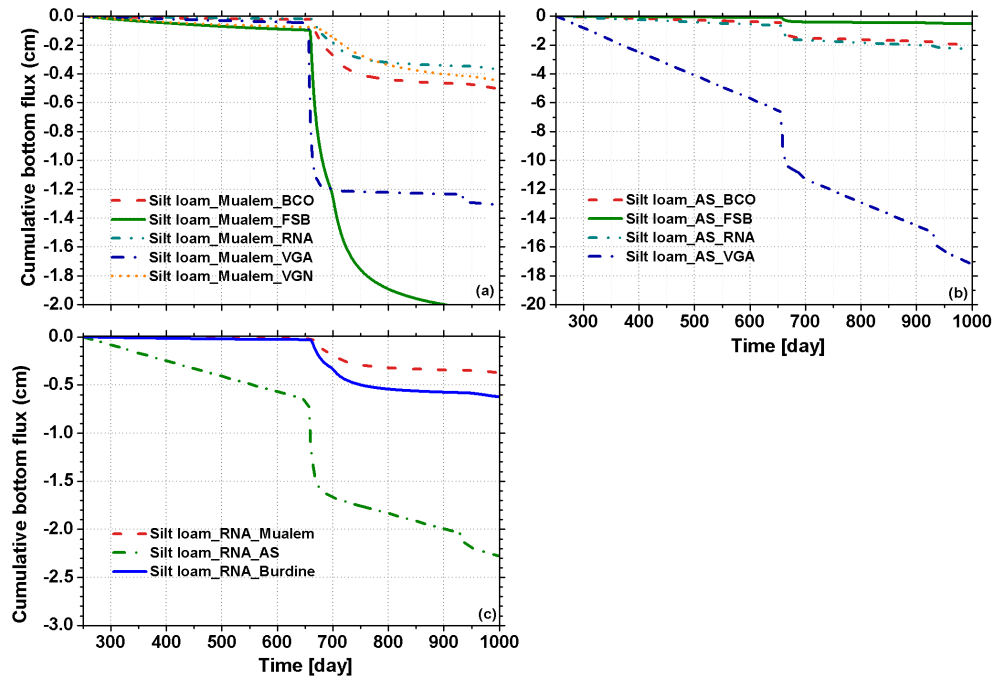


Figure 13. Cumulative bottom fluxes from a silt loam profile for all combinations of parameterizations (see Table 1) and Mualem's (1976) (a) and Alexander and Skaggs' (1986) conductivity functions (b), and for the RNA parameterization with all three conductivity functions (c).

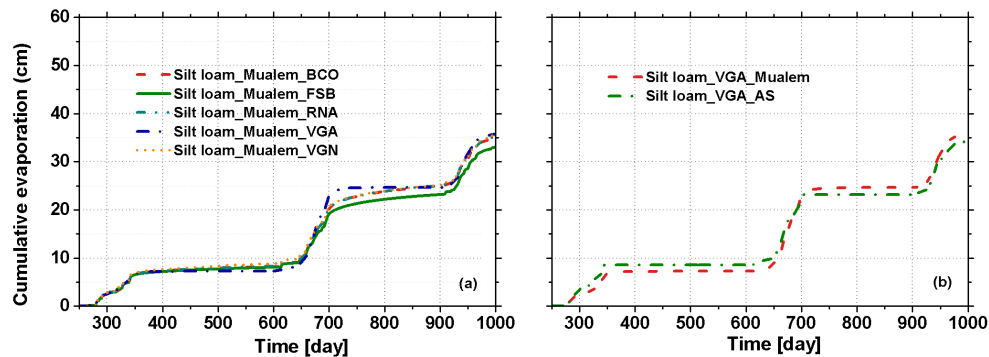


Figure 14. Cumulative evaporation from a silt loam profile for all parameterizations (see Table 1) with Mualem's (1976) conductivity function (a) and the VGA parameterization with conductivity functions according to Mualem (1976) and Alexander and Skaggs (1986) (b).

This resulted in a rapid and unrealistically strong response to changes in atmospheric forcings even at 1 m depth, as shown in our simulation study.

The simulations with different parameterizations showed that under the given boundary conditions the choice of the parameterization had a modest effect on evaporation but strongly affected the partitioning between soil water storage and deep percolation. The uncritical use of a default soil hydraulic parameterization or selection of a parameterization solely based on the quality of the fit to soil water retention data points entails the risk of an incomplete appreciation of the potential errors of the water fluxes occurring in the modeled soil. This points to the importance of carefully

considering the soil hydraulic parameterization to be used for long-term water balance studies. Such studies typically aim to determine or predict the variation of seasonal water availability to plants or long-term groundwater recharge to assess the sustainability of extractions from an underlying aquifer. If at all possible, observations during dynamic flow (water contents, matric potentials, fluxes) should be included in the parameterization selection process. In this context it would be interesting to see if parameter-estimation processes based on inverse modeling of a nonsteady unsaturated flow experiment would lead to a different choice of parameterization than fitting parameters to data points obtained at hydrostatic equilibrium. This requires the inclusion of all the parametric

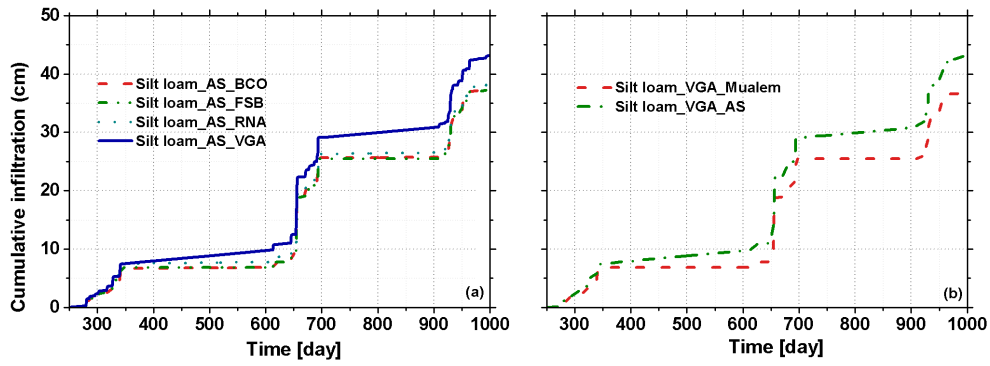


Figure 15. Cumulative infiltration from a silt loam profile for four parameterizations (see Table 1) with the Alexander and Skaggs (1986) conductivity function (a) and for the VGA parameterizations with conductivity functions according to Mualem (1976) and Alexander and Skaggs (1986) (b).

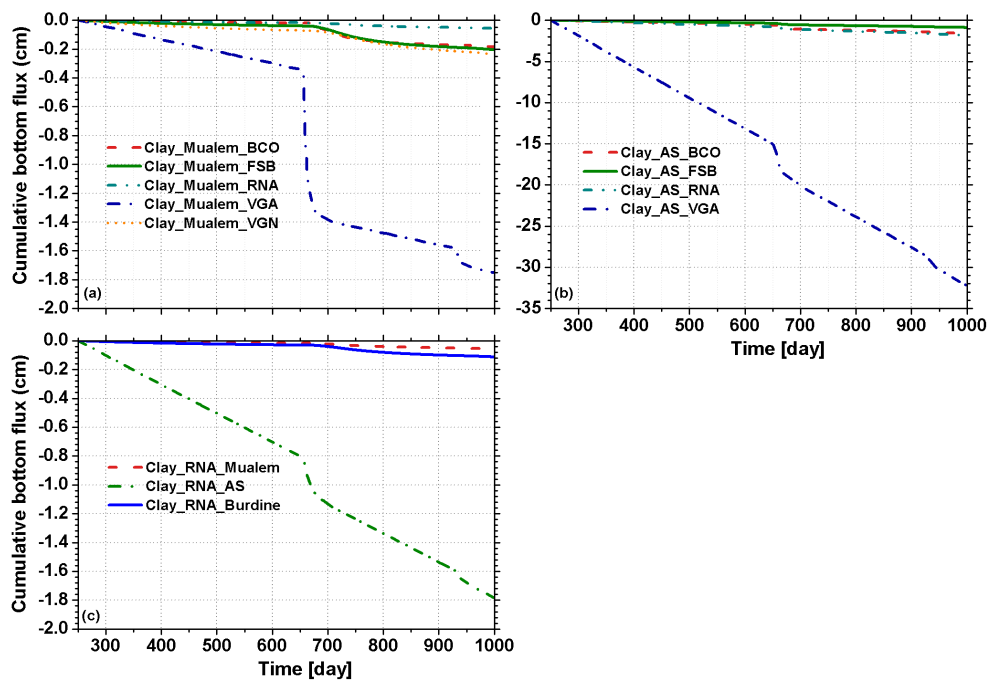


Figure 16. As in Fig. 13, for clay.

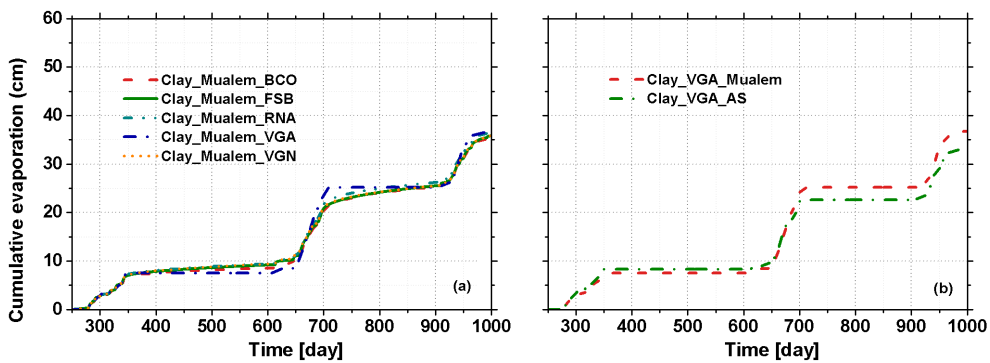


Figure 17. As in Fig. 14, for clay.

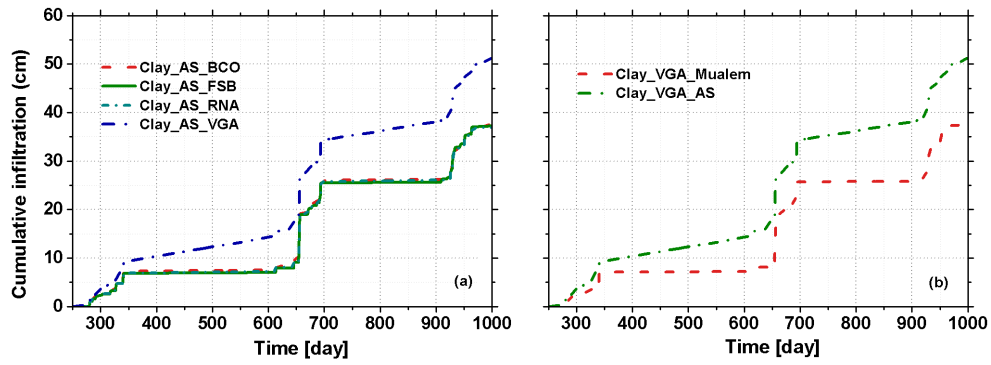


Figure 18. As in Fig. 15, for clay.

expressions of interest in the numerical solvers of Richards' equation capable of running in parameter estimation mode.

Code and data availability. The parameter optimization code is available upon request from Gerrit Huibert de Rooij. At a later time we intend to make the code available through a website.

Appendix A: List of variables

Variables	Dimensions	Properties, and equation to which the variable pertains (where applicable)
A_1	L^{-2}	Constant, Eq. (S3)
A_2	–	Constant, Eq. (S8a)
$B(h)$	L^n	Function simplifying notation, Eq. (S7c)
b	–	Shape parameter, Eq. (S21)
C	–	Constant simplifying notation, Eq. (S7c)
c_1	–	Constant, Eq. (S10a)
c_2	–	Constant, Eq. (S11a)
d_θ	Varies	Vector of length q_θ of squared differences between observations and fits, Eq. (27)
$E(h)$	$L^{-\kappa}$	Function simplifying notation, Eq. (S9e)
F	L^λ	Constant simplifying notation, Eq. (S9e)
$F_R(x_{p,R})$	–	Objective function
G	–	Constant simplifying notation, Eq. (S12c)
g_0, g_1	–	Fitting parameter, Eq. (S15a)
H	L	Sample height
h	L	Matric potential
h_a	L	Matric potential at which the soil reaches the maximum adsorbed water content
h_{ae}	L	Air-entry value of the soil
h_c	L	Fitting parameter
h_d	L	Pressure head at oven dryness
h_i	L	Matric potential at the inflection point
h_j	L	Pressure head at junction point
h_m	–	Fitting parameter representing the matric potential at median pore size
h_s	L	Minimum capillary height
I	–	Constant simplifying notation, Eq. (S12c)
J	$L^{-\lambda-\kappa}$	Function simplifying notation, Eq. (S12c)
j	–	Counter
K	$L T^{-1}$	Unsaturated hydraulic conductivity
K_s	$L T^{-1}$	Saturated hydraulic conductivity
L	–	Constant simplifying notation, Eq. (S14c)
M_1	–	Constant simplifying notation, Eq. (S14c)
M_2	–	Constant simplifying notation, Eq. (S14g)
m	–	Shape parameter of $\theta(h)$
n	–	Shape parameter of $\theta(h)$
$P(h)$	–	Function simplifying notation, Eq. (S14c)
R	–	Iteration step
R_{\max}	–	Maximum number of iterations
S	$L^3 L^{-3}$	Variable running from 0 to S_e
S^{ad}	–	Adsorbed water, Eq. (S16)
S^{cap}	–	Capillary water, Eq. (S16)
S_e	–	Degree of saturation
T	–	Indicates that the vector is transposed
w	–	Weighting factor ranging between 0 and 1, Eq. (S16)
$w_{\theta,R}$	–	Weight factor vector
$w_{R,i}$	–	Individual weighting factor in $w_{\theta,R}$
x	Varies	Integration variable
\mathbf{x}	Varies	Parameter vector
\mathbf{x}_f	Varies	Vector of nonfitted parameters
$\mathbf{x}_{p,R}$	Varies	Vector of fitted parameters
Y	–	Number of complexes
α	L^{-1}	Shape parameter of $\theta(h)$
β	–	Constant
γ	–	Shape parameter of $K(h)$

Variables	Dimensions	Properties, and equation to which the variable pertains (where applicable)
ζ_1	–	Constant, Eq. (S10a)
ζ_2	–	Constant, Eq. (S11a)
η	–	Fitting parameter
θ	$L^3 L^{-3}$	Volumetric water content
θ_a	$L^3 L^{-3}$	Curve fitting parameter representing the volumetric water content when $h = -1$ cm
θ_i	$L^3 L^{-3}$	i th observation of the volumetric water content
θ_j	$L^3 L^{-3}$	Volumetric water content at junction point
θ_m	$L^3 L^{-3}$	Water content at h_m
θ_r	$L^3 L^{-3}$	Residual water content
θ_s	$L^3 L^{-3}$	Saturated water content
κ	–	Shape parameter of $K(h)$
λ	–	Fitting parameter of $\theta(h)$
σ	–	Fitting parameter that characterizes the width of the pore size distribution
$\sigma_{h,i}, \sigma_{\theta,i}$	–	Error standard deviations for the i th matric potential and the i th water content, respectively
$\sigma_{h,i}^*, \sigma_{\theta,i}^*$	–	Scaled values of $\sigma_{h,i}, \sigma_{\theta,i}$
$\sigma_{i,R}^*$	–	Scaled standard deviation of (h_i, θ_i) during iteration R
τ	–	Shape parameter of $K(h)$

The Supplement related to this article is available online at <https://doi.org/10.5194/hess-22-1193-2018-supplement>.

Author contributions. RM gathered the soil hydraulic functions from the literature. RM and GHdR carried out the parameter optimization runs with the SCE-based code. RM and GHdR designed the test problem (column size, initial and boundary conditions) for the test simulations with HYDRUS-1D. RM set up, ran, and analyzed these model simulations. GHdR wrote the shell of the optimization code, selected the UNSODA soils, and carried out the mathematical analysis of the soil hydraulic functions. HM carried out the experiments that generated the data for the soils used in the simulations. JM wrote the SCE parameter optimization code. RM and GHdR wrote the paper. All authors were involved in checking and improving the paper.

Competing interests. Gerrit Huibert de Rooij is a member of the HESS Editorial Board.

The article processing charges for this open-access publication were covered by a Research Centre of the Helmholtz Association.

Edited by: Alberto Guadagnini

Reviewed by: Antonio Coppola and four anonymous referees

References

- Alexander, L. and Skaggs, R. W.: Predicting unsaturated hydraulic conductivity from the soil water characteristic, *Trans. Am. Soc. Agric. Eng.*, 29, 176–184, 1986.
- Assouline, S. and Or, D.: Conceptual and parametric representation of soil hydraulic properties: a review, *Vadose Zone J.*, 12, <https://doi.org/10.2136/vzj2013.07.0121>, 2013.
- Barnes, C. J. and Turner, J. V.: Isotopic exchange in soil water, in: *Isotope tracers in catchment hydrology*, edited by: Kendall, C. and McDonnell, J. J., Elsevier, Amsterdam, 839 pp., 137–163, 1998.
- Behrangi, A., Khakbaz, B., Vrugt, J. A., Duan, Q., and Sorooshian, S.: comment on “Dynamically dimensioned search algorithm for computationally efficient watershed model calibration” by Tolson, B.A., and Shoemaker, C. A., *Water Resour. Res.*, 44, W12603, <https://doi.org/10.1029/2007WR006429>, 2008.
- Bradley, R. S.: Polymolecular adsorbed films. Part I. The adsorption of argon on salt crystals at low temperatures, and the determination of surface fields, *J. Chem. Soc. (Resumed)*, 1467–1474, <https://doi.org/10.1039/JR9360001467>, 1936.
- Brooks, R. H. and Corey, A. T.: Hydraulic properties of porous media, Colorado State University, Hydrology Paper No. 3, 27 pp., 1964.
- Burdine, N. T.: Relative permeability calculations from pore size distribution data, *Trans. Am. Inst. Min. Metall. Pet. Eng.*, 198, 71–81, 1953.
- Campbell, G. S. and Shiozawa, S.: Prediction of hydraulic properties of soils using particle-size distribution and bulk density data, in: *Indirect methods for estimating the hydraulic properties of unsaturated soils*, edited by: van Genuchten, M. Th., Leij, F. J., and Lund, L. J., University of California, Riverside, 317–328, 1992.
- Coppola, A.: Unimodal and bimodal descriptions of hydraulic properties for aggregated soils, *Soil Sci. Soc. Am. J.*, 64, 1252–1262, 2000.
- Coppola, A., Basile, A., Comegna, A., and Lamaddalena, N.: Monte Carlo analysis of field water flow comparing uni- and bimodal effective hydraulic parameters for structured soil, *J. Contam. Hydrol.*, 104, 153–165, <https://doi.org/10.1016/j.jconhyd.2008.09.007>, 2009.
- Cornelis, W. M., Khlosi, M., Hartmann, R., Van Meirvenne, M., and De Vos, B.: Comparison of unimodal analytical expressions for the soil-water retention curve, *Soil Sci. Soc. Am. J.*, 69, 1902–1911, <https://doi.org/10.2136/sssaj2004.0238>, 2005.
- de Vries, J. J. and Simmers, I.: Groundwater recharge: an overview of processes and challenges, *Hydrogeol. J.*, 10, 5–17, <https://doi.org/10.1007/s10040-001-0171-7>, 2002.
- Duan, Q., Sorooshian, S., and Gupta, V.: Effective and efficient global optimization for conceptual rainfall-runoff models, *Water Resour. Res.*, 28, 1015–1031, 1992.
- Durner, W.: Hydraulic conductivity estimation for soils with heterogeneous pore structure, *Water Resour. Res.* 30, 211–223, 1994.
- Durner, W. and Flühler, H.: Soil hydraulic properties, *Encyclopedia of Hydrological Sciences*, John Wiley & Sons, Ltd, <https://doi.org/10.1002/0470848944.hsa077c>, 2005.
- Fayer, M. J. and Simmons, C. S.: Modified soil water retention functions for all matric suctions, *Water Resour. Res.*, 31, 1233–1238, 1995.
- Groenevelt, P. H. and Grant, C. D.: A new model for the soil-water retention curve that solves the problem of residual water contents, *Eur. J. Soil Sci.*, 55, 479–485, <https://doi.org/10.1111/j.1365-2389.2004.00617.x>, 2004.
- Hoffmann-Riem, H., van Genuchten, M. Th., and Flühler, H.: General model for the hydraulic conductivity of unsaturated soils, in: *Proceedings of the international workshop on characterization and measurement of the hydraulic properties of unsaturated porous media*, edited by: van Genuchten, M. Th., Leij, F. J., and Wu, L., Riverside, California, 22–24 October 1997, Part 1. U. S. Salinity Laboratory, ARS, US Dept. of Agriculture and Dept. of Environ. Sci., University California, Riverside, California, 31–42, 1999.
- Hollenbeck, K. J. and Jensen, K. H.: Maximum-likelihood estimation of unsaturated hydraulic parameters, *J. Hydrol.*, 210, 192–205, 1998.
- Hollenbeck, K. J., Šimůnek, J., and van Genuchten, M. Th.: RETMCL: Incorporating maximum-likelihood estimation principles in the RETC soil hydraulic parameter estimation code, *Comput. Geosci.*, 26, 319–327, 2000.
- Hutson, J. L. and Cass, A.: A retentive functions for use in soil-water simulation models, *J. Soil Sci.*, 38, 105–113, 1987.
- Iden, S. C. and Durner, W.: Free-form estimation of soil hydraulic properties using Wind’s method, *Eur. J. Soil Sci.*, 59, 1365–2389, <https://doi.org/10.1111/j.1365-2389.2008.01068.x>, 2008.
- Iden, S. C., Peters, A., and Durner, W.: Improving prediction of hydraulic conductivity by constraining capillary bundle mod-

- els to a maximum pore size, *Adv. Water Resour.*, 85, 86–92, <https://doi.org/10.1016/j.advwatres.2015.09.005>, 2015.
- Ippisch, O., Vogel, H.-J., and Bastian, P.: Validity limits for the van Genuchten-Mualem model and implications for parameter estimation and numerical simulation, *Adv. Water Resour.*, 29, 1780–1789, <https://doi.org/10.1016/j.advwatres.2005.12.011>, 2006.
- Jarvis, N. J., Zavattaro, L., Rajkai, K., Reynolds, W. D., Olsen, P. A., McGechan, M., Mecke, M., Mohanty, B., Leeds-Harrison, P. B., and Jacques, D.: Indirect estimation of near-saturated hydraulic conductivity from readily available soil information, *Geoderma*, 108, 1–17, 2002.
- Khlosi, M., Cornelis, W. M., Douaik, A., van Genuchten, M. Th., and Gabriels, D.: Performance evaluation of models that describe the soil water retention curve between saturation and oven dryness, *Vadose Zone J.*, 7, 87–96, <https://doi.org/10.2136/vzj2007.0099>, 2008.
- Kirkpatrick, S., Gelatt, C. D., and Vecchi, M. P.: Optimization by simulated annealing, *Science*, 220, 671–680, <https://doi.org/10.1126/science.220.4598.671>, 1983.
- Klute, A.: Water retention: Laboratory methods, in: *Methods of soil analysis. Part 1. Physical and mineralogical methods*, edited by: Klute, A., Second Edn., American Society of Agronomy, Inc., Soil Science Society of America, Inc. Madison, Wisconsin, USA, 635–662, 1986.
- Kosugi, K.: Three-parameter lognormal distribution model for soil water retention, *Water Resour. Res.*, 30, 891–901, <https://doi.org/10.1029/93WR02931>, 1994.
- Kosugi, K.: Lognormal distribution model for unsaturated soil hydraulic properties, *Water Resour. Res.*, 32, 2697–2703, 1996.
- Kosugi, K.: General model for unsaturated hydraulic conductivity for soils with lognormal pore-size distribution, *Soil Sci. Soc. Am. J.*, 63, 270–277, 1999.
- Kosugi, K., Hopmans, J. W., and Dane, J. H.: Water retention and Storage. Parametric models, in: *Methods of soil analysis. Part 4. Physical methods*, edited by: Dane, J. H. and Topp, G. C., American Society of Agronomy, Inc. Soil Science Society of America, Inc. Madison, Wisconsin, USA, 739–757, 2002.
- Lebeau, M. and Konrad, J.-M.: A new capillary and thin film flow model for predicting the hydraulic conductivity of unsaturated porous media, *Water Resour. Res.*, 46, W12554, <https://doi.org/10.1029/2010WR009092>, 2010.
- Leij, F. J., Russell, W. B., and Lesch, S. M.: Closed-form expressions for water retention and conductivity data, *Ground Water*, 35, 848–858, 1997.
- Liu, H. H. and Dane, J. H.: Improved computational procedure for retention relations of immiscible fluids using pressure cells, *Soil Sci. Soc. Am. J.*, 59, 1520–1524, 1995.
- Mualem, Y.: A new model for predicting the hydraulic conductivity of unsaturated porous media, *Water Resour. Res.*, 12, 513–521, 1976.
- Mualem, Y.: Modeling the hydraulic conductivity of unsaturated porous media, in: *Indirect methods for estimating the hydraulic properties of unsaturated soils*, edited by: van Genuchten, M. Th., Leij, F. J., and Lund, L. J., University of California, Riverside, 15–36, 1992.
- Mualem, Y. and Dagan, G.: Hydraulic conductivity of soils: unified approach to statistical models, *Soil Sci. Soc. Am. J.*, 42, 392–395, 1978.
- Nasta, P., Vrugt, J. A., and Romano, N.: Prediction of the saturated hydraulic conductivity from Brooks and Corey’s water retention parameters, *Water Resour. Res.*, 49, 2918–2925, <https://doi.org/10.1002/wrcr.20269>, 2013.
- National Agricultural Library: <https://data.nal.usda.gov/dataset/unsoda-20-unsaturated-soil-hydraulic-database-database-and-program-indirect-methods-estimating-unsaturated-hydraulic-properties>, last access: 7 February 2018.
- National centers for environmental information: <http://www.ncdc.noaa.gov/cdo-web/>, last access: 11 September 2017.
- Nemes, A., Schaap, M. G., Leij, F. J., and Wösten, J. H. M.: Description of the unsaturated soil hydraulic database UNSODA version 2.0, *J. Hydrol.*, 251, 152–162, [https://doi.org/10.1016/S0022-1694\(01\)00465-6](https://doi.org/10.1016/S0022-1694(01)00465-6), 2001.
- Peters, A.: Reply to comment by Iden, D. and Durner, W. on “Simple consistent models for water retention and hydraulic conductivity in the complete moisture range”, *Water Resour. Res.*, 50, 7535–7539, <https://doi.org/10.1002/2014WR016107>, 2014.
- Peters, A. and Durner, W.: Simplified evaporation method for determining soil hydraulic properties, *J. Hydrol.*, 356, 147–162, 2008.
- Pollacco, J. A. P., Nasta, P., Soria-Ugalde, J. M., Angulo-Jaramillo, R., Lassabatere, L., Mohanty, B. P., and Romano, N.: Reduction of feasible parameter space of the inverted hydraulic parameter sets for Kosugi model, *Soil Sci.*, 178, 267–280, <https://doi.org/10.1097/SS.0b013e3182a2da21>, 2013.
- Pollacco, J. A. P., Webb, T., McNeill, S., Hu, W., Carrick, S., Hewitt, A., and Lilburne, L.: Saturated hydraulic conductivity model computed from bimodal water retention curves for a range of New Zealand soils, *Hydrol. Earth Syst. Sci.*, 21, 2725–2737, <https://doi.org/10.5194/hess-21-2725-2017>, 2017.
- Press, W. H., Teukolsky, S. A., Vetterling, W. T., and Flannery, B. P.: *Numerical recipes in Fortran. The art of scientific computing*, 2nd Edn., Cambridge University Press, Cambridge, UK, 1992.
- Priesack, E. and Durner, W.: Closed-form expression for the multimodal unsaturated conductivity function, *Vadose Zone J.*, 5, 121–124, <https://doi.org/10.2136/vzj2005.0066>, 2006.
- Raats, P. A. C.: A superclass of soils, in: *Indirect methods for estimating the hydraulic properties of unsaturated soils*, edited by: van Genuchten, M. Th., Leij, F. J., and Lund, L. J., University of California, Riverside, 45–51, 1992.
- Romano, N., Nasta, P., Severino, G., and Hopmans, J. W.: Using bimodal lognormal functions to describe soil hydraulic properties, *Soil Sci. Soc. Am. J.*, 75, 468–480, <https://doi.org/10.2136/sssaj2010.0084>, 2011.
- Rossi, C. and Nimmo, J. R.: Modeling of soil water retention from saturation to oven dryness, *Water Resour. Res.*, 30, 701–708, 1994.
- Scanlon, B. R., Keese, K. E., Flint, A. L., Flint, L. E., Gaye, C. B., Edmunds, W. M., and Simmers, I.: Global synthesis of groundwater recharges in semiarid and arid regions, *Hydrol. Process.*, 20, 3335–3370, <https://doi.org/10.1002/hyp.6335>, 2006.
- Schaap, M. G. and Leij, F. J.: Improved prediction of unsaturated hydraulic conductivity with the Mualem-van Genuchten model, *Soil Sci. Soc. Am. J.*, 64, 843–851, 2000.
- Schelle, H., Heise, L., Jänicke, K., and Durner, W.: Water retention characteristics of soils over the whole moisture range: a comparison of laboratory methods, *Eur. J. Soil Sci.*, 64, 814–821, 2013.
- Schindler, U., von Unold, G., Durner, W., and Mueller, L.: Recent progress in measuring soil hydraulic properties, in: *Pro-*

- ceedings of the International Conference on Environment and Civil Engineering, 24–25 April 2015, Pattaya, Thailand, 47–52, <https://doi.org/10.15242/IAE.IAE0415401>, 2015.
- Šimůnek, J., Šejna, M., Saito, H., Sakai, M., and van Genuchten, M. Th.: The HYDRUS-1D software package for simulating the one-dimensional movement of water, heat, and multiple solutes in variably-saturated media, Version 4.17, Dept. Env. Sci., University California, Riverside, California, USA, 2013.
- Tolson, B. A. and Shoemaker, C. A.: Dynamically dimensioned search algorithm for computationally efficient watershed model calibration, *Water Resour. Res.*, 43, W01413, <https://doi.org/10.1029/2005WR004723>, 2007.
- Tuller, M. and Or, D.: Hydraulic conductivity of variably saturated porous media: Film and corner flow in angular pore space, *Water Resour. Res.*, 37, 1257–1276, <https://doi.org/10.1029/2000WR900328>, 2001.
- Twarakavi, N. K. C., Šimůnek, J., and Schaap, M. G.: Can texture-based classification optimally classify soils with respect to soil hydraulics?, *Water Resour. Res.*, 46, W01501, <https://doi.org/10.1029/2009WR007939>, 2010.
- Tyler, S. W. and Wheatcraft, S. W.: Fractal processes in soil water retention, *Water Resour. Res.*, 26, 1047–1054, 1990.
- UMS: HYPROP-Fit User Manual, UMS GmbH, Munich, Germany, <http://www.ums-muc.de/en/home/> (last access: 7 February 2018), 2015.
- UNDP: Human Development Report 2006. Beyond scarcity: power, poverty and the global water crisis, United Nations development programme, New York, 422 pp., 2006.
- UN-Water, FAO: Coping with water scarcity, Challenge of the twenty-first century, 29 pp., 2007.
- van Genuchten, M. Th.: A closed-form equation for predicting the hydraulic conductivity for unsaturated soils, *Soil Sci. Soc. Am. J.*, 44, 892–898, 1980.
- Vogel, T., van Genuchten, M. Th., and Cislerova, M.: Effect of the shape of the soil hydraulic functions near saturation on variably-saturated flow predictions, *Adv. Water Resour.*, 24, 133–144, 2001.